

Hypoxia-induced downregulation of PGK1 crotonylation promotes tumorigenesis by coordinating glycolysis and the TCA cycle

Received: 10 August 2023

Accepted: 2 August 2024

Published online: 12 August 2024

Check for updates

Zihao Guo^{1,2}, Yang Zhang¹, Haoyue Wang¹, Liming Liao³, Lingdi Ma¹, Yiliang Zhao², Ronghui Yang¹, Xuexue Li¹, Jing Niu², Qiaoyun Chu², Yanxia Fu², Binghui Li^{1,2,4}✉ & Chuanzhen Yang^{1,2,3}✉

Protein post-translational modifications (PTMs) are crucial for cancer cells to adapt to hypoxia; however, the functional significance of lysine crotonylation (Kcr) in hypoxia remains unclear. Herein we report a quantitative proteomics analysis of global crotonylome under normoxia and hypoxia, and demonstrate 128 Kcr site alterations across 101 proteins in MDA-MB231 cells. Specifically, we observe a significant decrease in K131cr, K156cr and K220cr of phosphoglycerate kinase 1 (PGK1) upon hypoxia. Enoyl-CoA hydratase 1 (ECHS1) is upregulated and interacts with PGK1, leading to the downregulation of PGK1 Kcr under hypoxia. Abolishment of PGK1 Kcr promotes glycolysis and suppresses mitochondrial pyruvate metabolism by activating pyruvate dehydrogenase kinase 1 (PDHK1). A low PGK1 K131cr level is correlated with malignancy and poor prognosis of breast cancer. Our findings show that PGK1 Kcr is a signal in coordinating glycolysis and the tricarboxylic acid (TCA) cycle and may serve as a diagnostic indicator for breast cancer.

Post-translational modifications (PTMs) increase the protein structure and function diversity by adding covalent chemical adducts to proteins, thereby regulating various biological processes and influencing the pathophysiologic progression of diseases, including cancer^{1–3}. These modifications, such as acetylation, phosphorylation, and ubiquitination at specific sites in proteins, have been extensively studied^{4–6}. With the rapid advances in protein mass spectrometry (MS), more types of PTMs have been identified^{7,8}. Lysine crotonylation (Kcr) has been shown to be a type of histone protein PTM by Tan et al.⁹, which is frequently enriched at histones near gene promoters and enhancers. Crotonyl-coenzyme A (CoA) is generated via fatty acid β -oxidation, or lysine or tryptophan catabolism. Crotonate can also be converted into crotonyl-CoA. Crotonyl-CoA contains a four-carbon acyl chain and a unique C–C π -bond. Crotonylation occurs primarily on the ϵ -amino group of lysine and is dynamically regulated by writers and

erasers. Histone acetyltransferases (HATs), including p300, PCAF, GCN5, and MOF, also act as the writers to catalyze lysine crotonylation, whereas the histone deacetylases, HDAC1/2/3/8 and SIRT1/2/3, function as erasers to remove the crotonyl group^{10–14}. Other regulators, including CDYL, ACSS2, and ECHS1, affect crotonylation by influencing crotonyl-CoA availability^{15–17}. In addition to histones, crotonyl modifications also occur in non-histone proteins^{18,19}. A significant proportion of crotonylated proteins are involved in metabolism¹⁸; however, the effects of crotonylation on metabolic-related protein function and the underlying mechanism remain to be elucidated.

Proliferating cancer cells require a high rate of glycolysis to produce energy and secrete most of the glucose-derived carbon as lactate, despite the availability of oxygen. This process is termed aerobic glycolysis^{20,21}. Although glycolysis is an inefficient way to generate ATP compared to mitochondrial oxidative phosphorylation, cancer cells

¹Beijing Institute of Hepatology, Beijing Youan Hospital, Capital Medical University, Beijing 100069, China. ²Department of Biochemistry and Molecular Biology, School of Basic Medical Sciences, Capital Medical University, Beijing 100069, China. ³Westlake Four-Dimensional Dynamic Metabolomics (Meta4D) Laboratory, Westlake Laboratory of Life Sciences and Biomedicine, Hangzhou 310024, China. ⁴Department of Cancer Cell Biology and National Clinical Research Center for Cancer, Tianjin Medical University Cancer Institute and Hospital, Tianjin 300060, China. ✉e-mail: bli@ccmu.edu.cn; yangchuanzhen@westlake.edu.cn

gain other advantages, including meeting the biosynthetic requirements for uncontrolled proliferation and maintaining redox capacity^{22,23}. Hypoxia is a hallmark of solid tumors because oxygen consumption exceeds supply^{24,25}. To adapt to hypoxia, mitochondrial pyruvate metabolism is suppressed in cancer cells. Under hypoxic conditions, hypoxia-inducible factor-1 alpha (HIF-1 α) upregulates pyruvate dehydrogenase kinase 1 (PDHK1 or PDK1) via transcription. PDHK1 phosphorylates the E1 α subunit of pyruvate dehydrogenase (PDH), which converts pyruvate to acetyl-coenzyme A (acetyl-CoA), thus inhibiting its activity, and limiting the entry of acetyl-CoA into the tricarboxylic acid (TCA) cycle and subsequent mitochondrial respiration^{26,27}. The accumulated pyruvate is then transformed to lactate by lactate dehydrogenase (LDH) in the cytosol. This hypoxia-induced metabolic switch is indispensable for attenuating mitochondrial ROS production and maintaining cellular ATP.

In this study, we use a quantitative proteomics method to analyze the global crotonylome in MDA-MB231 cells cultured under normoxia and hypoxia. We identify 3971 Kcr sites across 1241 proteins. Quantitative comparison of crotonylome between normoxic and hypoxic groups shows that 128 Kcr sites are altered in response to hypoxia. Notably, phosphoglycerate kinase 1 (PGK1) K131cr, K156cr, and K220cr are significantly decreased upon hypoxia. We demonstrate that ECHS1 interacts with PGK1 and downregulates the PGK1 Kcr under hypoxia. Blocking the PGK1 Kcr enhances glycolysis and suppresses mitochondrial pyruvate metabolism by activating PDHK1, thereby promoting tumorigenesis. Furthermore, a low PGK1 Kcr level is associated with malignancy and poor prognosis of breast cancer.

Results

The global crotonylome demonstrates downregulation of PGK1 crotonylation under hypoxia

To determine the effects of hypoxia on global protein crotonylation, we used tandem mass tag (TMT) labeling, immunoaffinity enrichment, and liquid chromatography-tandem mass spectrometry (LC-MS/MS) to measure the levels of the MDA-MB231 cell Kcr proteins when cultured under hypoxia and normoxia (Fig. 1a). Hypoxia led to increased glucose consumption and lactate production, which was in agreement with previous reports (Fig. 1b)^{28,29}. We identified 3971 Kcr sites across 1241 proteins in MDA-MB231 cells, with 3231 Kcr sites across 1043 proteins quantified (Fig. 1c). A total of 128 Kcr sites in 101 proteins changed in response to hypoxia (Fig. 1d). The subcellular localization of these Kcr substrates was found mainly in the cytoplasm and nucleus (Fig. 1e). The protein enrichment analysis of the altered crotonylated proteins indicated that Kcr may impose effects on the monosaccharide catabolic process, carbohydrate catabolic process, and mitochondrial membrane permeability upon hypoxia (Fig. 1f). Additionally, a volcano plot showed that the PGK1 Kcr on the K131, K156, and K220 sites were significantly downregulated (Fig. 1g).

PGK1 plays a crucial role in glycolysis by catalyzing the conversion of 1,3-diphosphoglycerate (1,3-BPG) and ADP to 3-phosphoglycerate (3-PG) and ATP, which is the first ATP-generating step. To validate the crotonylome results, immunoprecipitation (IP) assays were performed, followed by immunoblotting with the antibody against Pan-Kcr. Indeed, the level of PGK1 Kcr decreased upon hypoxia in MDA-MB231 cells (Fig. 1h and Supplementary Fig. 1a). We also confirmed downregulation of PGK1 Kcr upon hypoxia in HEK293T and HCC1806 cells (Fig. 1i and Supplementary Fig. 1b–d). Crotonate and acetate could be converted to the cognate acyl-CoAs³⁰. The addition of crotonate, but not acetate, increased the level of PGK1 Kcr (Fig. 1j). Furthermore, we assessed the effect of crotonate supplementation on cellular crotonyl-CoA levels and PGK1 Kcr under normoxic and hypoxic conditions. Our results demonstrated that the addition of crotonate increased cellular crotonyl-CoA levels and PGK1 Kcr under normoxic conditions. However, this effect was abolished upon hypoxic treatment (Fig. 1k and

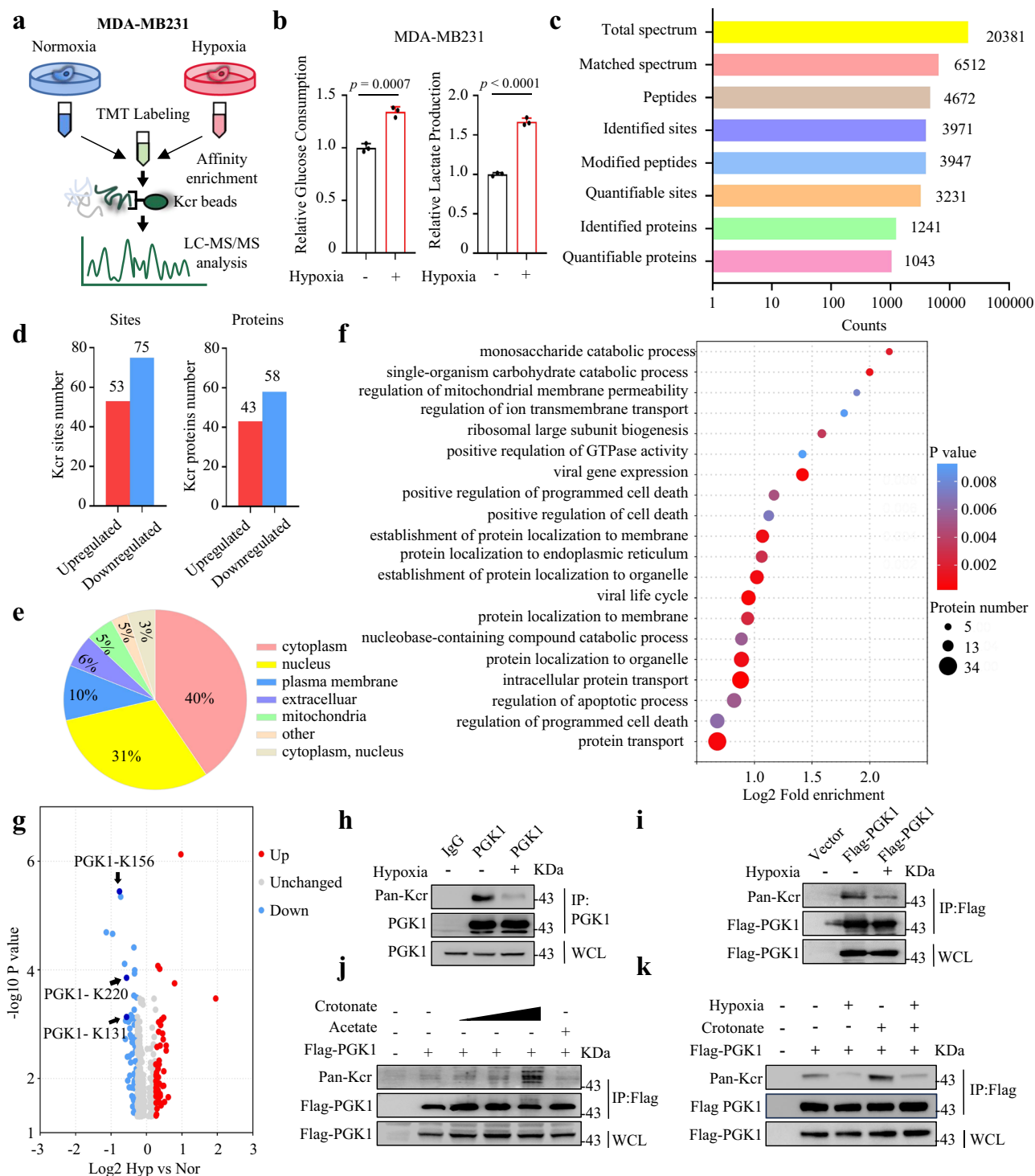
Supplementary Fig. 1e, f). Taken together, these findings suggest that PGK1 Kcr can be downregulated by hypoxia.

PGK1 Kcr at the K131, K156 and K220 sites decreases under hypoxia

To confirm PGK1 Kcr at the K131, K156, and K220 sites, we synthesized standard Kcr peptides, including FHVEEGK_{cr}GK, ASLSK_{cr}LGDVYVNDVAFGTAHR, and VADK_{cr}IQLINMLDK. We then compared their MS/MS spectra with the derived peptides from the MDA-MB231 cells. The results demonstrated that the *in vivo* derived PGK1 K131cr peptide, the synthetic standard PGK1 K131cr peptide, and the mixture of these two peptides exhibited nearly identical fragmentation patterns in tandem mass spectrometry, as well as similar retention times in liquid chromatography (Fig. 2a, b). Similar results were observed for PGK1 K156cr and K220cr (Supplementary Fig. 2a, b and Supplementary Fig. 3a, b). These data suggest that PGK1 is indeed crotonylated at the K131, K156, and K220 sites.

The crotonylome data indicated a reduction in PGK1 K131cr, K156cr, and K220cr by 0.676-, 0.589-, and 0.676-fold, respectively, under hypoxia, while other sites did not exhibit a significant change (Fig. 2c). The LC-MS/MS analysis confirmed the downregulation of PGK1 Kcr at these three sites (Supplementary Fig. 4a). Additionally, lactylation was observed on PGK1 at K131, which remained almost unaffected by hypoxic treatment (Supplementary Fig. 4a). Subsequently, IP assays were conducted to investigate other lysine PTMs on PGK1. The results demonstrated the presence of crotonylation on PGK1, while lactylation and acetylation were not detected (Supplementary Fig. 4b). Notably, although hypoxia led to an increase in protein modification by lactylation, lactylation on PGK1 was not observed, possibly due to the low intensity of PGK1 lactylation at K131 (Supplementary Fig. 4b). Given the relatively abundant presence of crotonylation on PGK1 and the consistent decrease in PGK1 Kcr induced by hypoxia, we focused on verifying and analyzing the functional implications of hypoxia-induced downregulation of PGK1 crotonylation. We then generated single-site mutants (K131R, K156R, and K220R), double-sites mutants (K131/156 R, K131/220 R, and K156/220 R), and triple-sites mutant (3KR-K131/156/220 R) by mutating the indicated PGK1 lysine (K) sites to arginine (R). IP analysis of HEK293T cells transfected with Flag-tagged wild-type (WT) or point mutants of PGK1 showed that PGK1 Kcr decreased with these single- or double-site mutants (Fig. 2d and Supplementary Fig. 4c). The PGK1 3KR mutant almost led to the complete abolishment of Kcr levels (Fig. 2d and Supplementary Fig. 4c). We also analyzed the conservation of these three PGK1 amino acid residues across different species and observed that all three sites were highly conserved through evolution (Fig. 2e).

To further validate the above results, we attempted to develop specific antibodies targeting PGK1 K131cr, K156cr, and K220cr. However, we successfully generated antibodies for K131cr and K156cr, but encountered difficulties in generating an antibody for K220cr due to challenges associated with the antigenicity, hydrophilicity, and spatial location of the amino acids surrounding K220. Then the specificity of PGK1 K131cr and K156cr antibodies was verified by performing dot blot assays. The results demonstrated that the PGK1 K131cr antibody selectively recognized the K131cr peptides, but not the K156cr, K220cr, K131a, K131ac, and the negative peptides (Fig. 2f and Supplementary Fig. 4d, e). Similarly, the PGK1 K156cr antibody displayed specific recognition of the K156cr peptides (Supplementary Fig. 4f). The IP analysis of HEK293T cells transfected with Flag-tagged PGK1 WT, K131R, or K156R demonstrated that K131R abolished the recognition by PGK1 K131cr antibody, whereas K156R did not affect the recognition by the indicated site-specific antibody, suggesting that only PGK1 K131cr antibody was available and specific (Fig. 2g and Supplementary Fig. 4g). We next examined whether PGK1 K131cr was responsive to hypoxia using this specific antibody recognizing K131cr. Our results



demonstrated that the PGK1 K131cr level decreased under hypoxia (Fig. 2h and Supplementary Fig. 4h). Moreover, the PGK1 K131cr level increased after crotonate treatment (Fig. 2i). Overall, these observations suggest that the PGK1 Kcr occurs at K131, K156, and K220 sites and is responsive to hypoxia.

ECHS1 mediates the downregulation of PGK1 cronylation under hypoxia

To determine the mechanism underlying the downregulation of PGK1 Kcr under hypoxia, IP-MS analysis was performed to identify the PGK1 interacting proteins. ECHS1 was immunoprecipitated by Flag-PGK1 (Fig. 3a). ECHS1 is a hydratase that catalyzes the hydrolyzation of

crotonyl-CoA, thereby potentially reducing intracellular crotonyl-CoA¹⁷. Consistently, we found ECHS1 converted crotonyl-CoA to 3-hydroxybutyryl-CoA in vitro (Supplementary Fig. 5a). Co-IP assays confirmed the interaction between PGK1 and ECHS1 in HEK293T and MDA-MB231 cells (Fig. 3b,c and Supplementary Fig. 5b). To assess whether PGK1 directly interacted with ECHS1, we purified GST-PGK1 and His-ECHS1 proteins in *Escherichia coli* and performed GST pull-down assays. The results showed a direct interaction between PGK1 and ECHS1 in vitro (Fig. 3d). Moreover, the Co-IP assays demonstrated that both wild-type and 3KR mutant of PGK1 bound to ECHS1, indicating PGK1-ECHS1 interaction remains unaffected by the cronylation of PGK1 (Fig. 3e). Analysis of the interface between PGK1 and

Fig. 1 | The global crotonylome reveals downregulation of PGK1 crotonylation under hypoxia. **a, b** Schematic illustration of TMT quantitative proteomics workflow to determine the levels of Kcr proteins in MDA-MB231 cells cultured under normoxic or hypoxic conditions for 12 h (**a**). Each group had 3 biologically independent samples. The relative levels of glucose consumption and lactate production were measured to confirm the effectiveness of hypoxia treatment (**b**). Data are shown as the mean \pm SD, $n = 3$ biologically independent samples (unpaired two-tailed Student's *t*-test). **c** Column chart showing the statistical proteins, peptides and sites information of TMT quantitative proteomics results. **d** Identified differential Kcr sites and proteins were counted. **e** Pie graph showing the sub-cellular distribution of identified Kcr differential proteins. **f** KEGG pathway enrichment of identified Kcr differential proteins. The dot size and color represent the protein number and the *p* value (unpaired two-tailed Student's *t*-test) of the corresponding pathway, respectively. **g** Volcano plots showing the quantification and *p* value (unpaired two-tailed Student's *t* test) of identified differential Kcr sites.

h MDA-MB231 cells were cultured under normoxia or hypoxia for 12 h and subjected to IP assays using anti-PGK1 or anti-IgG antibodies, followed by immunoblotting with pan anti-Kcr and anti-PGK1 antibodies. WCL, whole-cell lysate. **i** IP assays were performed with anti-Flag M2 beads using HEK293T cells expressing the Flag-tagged PGK1 cultured under normoxia or hypoxia for 12 h, followed by immunoblotting with pan anti-Kcr and anti-Flag antibodies. **j** HEK293T cells expressing Flag-tagged PGK1 were pretreated with 2.5, 5, or 10 mM sodium crotonate (pH 7.4) or 10 mM sodium acetate (pH 7.4) for 12 h. IP assays were performed with anti-Flag M2 beads, followed by immunoblotting with the indicated antibodies. **k** HEK293T cells expressing Flag-tagged PGK1 were pretreated with or without 10 mM sodium crotonate (pH 7.4) and subsequently cultured under normoxia or hypoxia for 12 h. IP assays were performed with anti-Flag M2 beads, followed by immunoblotting with the indicated antibodies. **b, h–k** Data were verified in at least three independent experiments. Source data are provided as a Source Data file.

ECHS1 in the AlphaFold2-predicted structure identified four putative ECHS1-binding sites in PGK1, including Lys133, Asn138, Lys139, and Lys144. We then generated a Flag-tagged PGK1 mutant with amino acid substitutions K133D, N138A, K139D, and K144D, and compared its interaction with ECHS1 to that of wild-type Flag-tagged PGK1. The results demonstrated that mutations in these four amino acids of PGK1 abolished its interaction with ECHS1. Interestingly, these mutations also led to an increase in PGK1 Kcr, indicating that the association between ECHS1 and PGK1 is necessary for the downregulation of PGK1 Kcr (Fig. 3f). We further determined whether ECHS1 affected PGK1 Kcr. Overexpression of ECHS1 in HEK293T cells also resulted in a reduction of PGK1 Kcr (Fig. 3g).

Next, we assessed whether hypoxia affected the interaction between PGK1 and ECHS1. Co-IP assays performed using MDA-MB231 and HCC1806 cells cultured under normoxia or hypoxia demonstrated that the PGK1-ECHS1 interaction was increased under hypoxia (Fig. 3h and Supplementary Fig. 5c–e). Subcellular co-localization analysis also confirmed the enhanced co-localization of PGK1 and ECHS1 (Fig. 3i). Moreover, we showed that ECHS1 protein expression increased after hypoxia treatment (Fig. 3j and Supplementary Fig. 5f–h). We then measured the abundance of ECHS1 mRNA in cells cultured under normoxia or hypoxia by quantitative real-time PCR and showed that ECHS1 transcription was upregulated by hypoxia (Supplementary Fig. 5i). The transcription factor, HIF-1 α , functions as a major regulator of hypoxia-inducible genes. Under normoxia, HIF-1 α interacts with Von Hippel-Lindau (VHL) tumor-suppressor protein, leading to degradation of HIF-1 α ; however, VHL tumor-suppressor protein dissociates from HIF-1 α under hypoxia, which results in stabilization of HIF-1 α ^{31,32}. To determine the role of HIF-1 α in regulating ECHS1 expression, we used the CRISPR/Cas9 system to knockout the VHL tumor-suppressor protein, which resulted in increased levels of HIF-1 α and ECHS1 (Supplementary Fig. 5j). Moreover, knockdown of HIF-1 α abolished the upregulation of ECHS1 at the mRNA and protein levels under hypoxia (Fig. 3k, l). The results of CUT&Tag qPCR assays also suggested that HIF-1 α was bound to the ECHS1 promoter under hypoxia (Fig. 3m, n).

Because ECHS1 could affect the intracellular level of crotonyl-CoA, we determined the contents of crotonyl-CoA in MDA-MB231/shScramble and MDA-MB231/shECHS1 cells cultured under normoxia or hypoxia. The intracellular level of crotonyl-CoA decreased under hypoxia, while knockdown of ECHS1 abolished this phenomenon (Supplementary Fig. 5k, l). As ECHS1 is known to localize in the mitochondria, we isolated both the mitochondrial and cytosolic fractions from MDA-MB231 cells to assess the levels of crotonyl-CoA in these different cellular compartments. Hypoxia resulted in a reduction in crotonyl-CoA levels in both the cytosol and mitochondria, which was also reversed by ECHS1 knockdown (Fig. 3o). Additionally, cell fractionation assays revealed that PGK1 primarily localized and undergoes crotonylation in the cytosol (Fig. 3p and Supplementary Fig. 5m). Under hypoxic conditions, there was a decrease in PGK1 Kcr levels in

the cytosol, accompanied by the translocation of cytosolic PGK1 to the mitochondria, where PGK1 Kcr levels were significantly lower (Fig. 3p and Supplementary Fig. 5m). Furthermore, IP analysis indicated that the PGK1 Kcr level decreased under hypoxia and depletion of ECHS1 completely eliminated the effect on PGK1 Kcr induced by hypoxia (Fig. 3q and Supplementary Fig. 5n). Taken together, these observations support the notion that ECHS1 is responsible for the reduction of PGK1 Kcr under hypoxia.

PCAF is the crotonyltransferase of PGK1 Kcr

Previous studies have reported that some HATs and HDACs also possess histone crotonyltransferase (HCT) and decrotonylase (HDCR) activity, and regulate substrate crotonylation. To identify the crotonyltransferase and decrotonylase for PGK1 Kcr, we transfected HEK293T cells with the indicated HATs and HDACs and performed IP analysis. The results showed that p300/CBP-associated factor (PCAF) interacted with PGK1 and promoted PGK1 Kcr (Fig. 4a and Supplementary Fig. 6a); however, we did not observe the decrotonylation effects of HDACs on PGK1 Kcr, although SIRT3 interacted with PGK1 (Fig. 4b and Supplementary Fig. 6b). Co-IP analysis further indicated that Flag-PGK1 or endogenous PGK1 interacted with PCAF in HEK293T, MDA-MB231 and HCC1806 cells (Fig. 4c, d and Supplementary Fig. 6c, d). Next, we performed GST pull-down experiments using GST-PGK1 purified from bacteria and HA-PCAF enriched from HEK293T cells. The result suggested that PCAF had a direct interaction with PGK1 (Fig. 4e). We then investigated whether PCAF could catalyze PGK1 Kcr in vitro. The results indicated that the addition of PCAF protein increased PGK1 Kcr (Fig. 4f); however, the inclusion of different amounts of PCAF protein did not further promote PGK1 Kcr (Fig. 4f). We next determined whether PCAF affected PGK1 Kcr in cells. Our result showed that overexpression of PCAF increased the PGK1 Kcr, while simultaneous expression of PCAF and ECHS1 resulted in a low level of PGK1 Kcr, indicating that the availability of crotonyl-CoA was critical for PGK1 Kcr (Fig. 4g). Co-IP analysis also confirmed that PCAF and PGK1 interaction was not affected by hypoxia (Fig. 4h and Supplementary Fig. 6e). In addition, cell fractionation assays showed that PCAF exhibited localization in the cytosol and mitochondria, suggesting a spatial basis for PGK1-PCAF interaction (Fig. 4i). These findings indicate that PCAF is the crotonyltransferase of PGK1 Kcr, but is independent for hypoxia-induced downregulation of PGK1 Kcr.

PGK1 crotonylation is indispensable for coordinating mitochondrial pyruvate metabolism and glycolysis

PGK1 is a key enzyme involved in glycolysis. We first examined whether crotonylation affected the glycolytic activity of PGK1. Flag-PGK1 WT or mutant enzymes expressed in HEK293T cells were enriched and used for the in vitro enzymatic assays. Our result showed that the glycolytic activity of PGK1 WT and point mutants K131R, K156R, K220R, and 3KR had no significant differences (Fig. 5a). Previous studies have shown

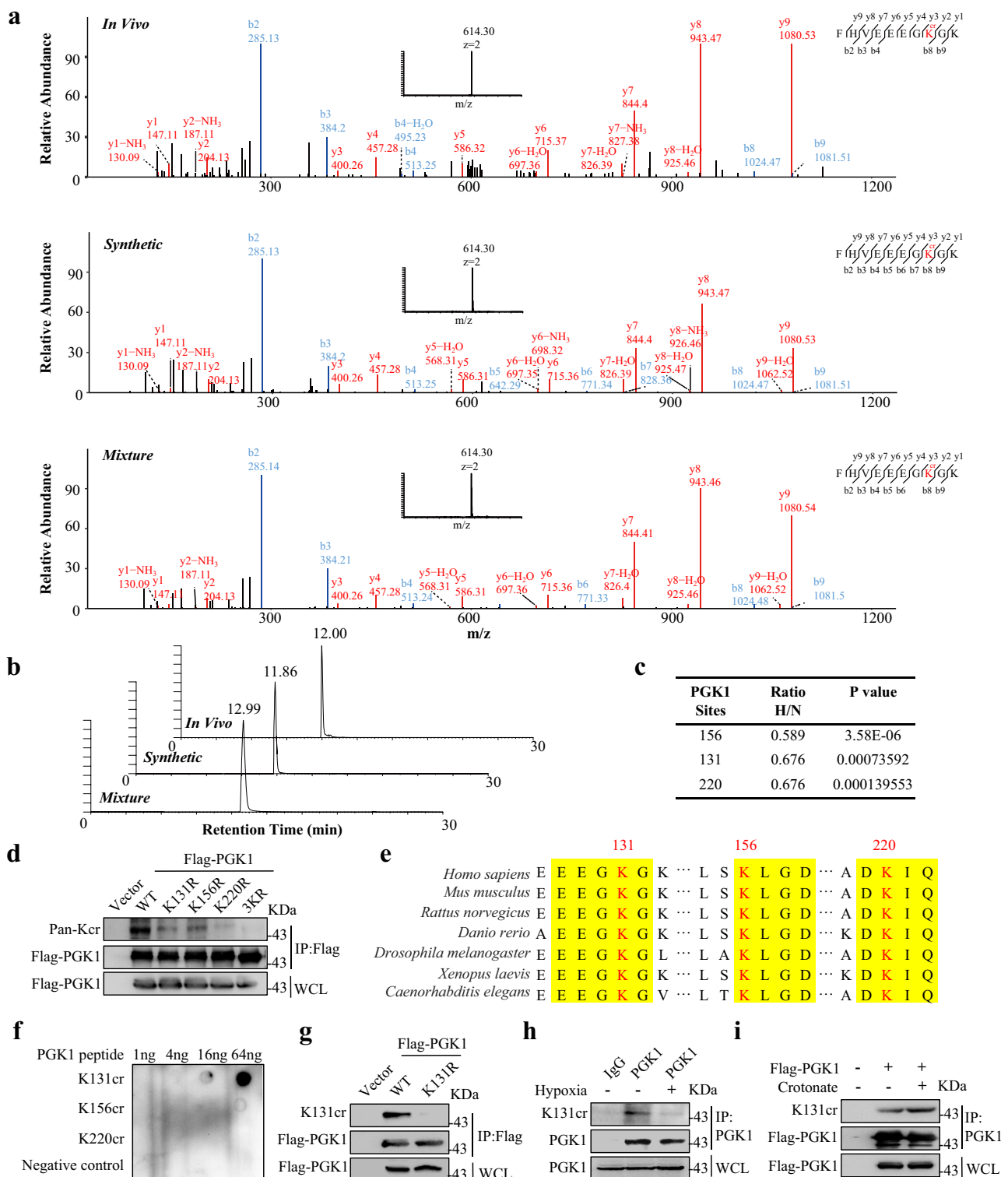
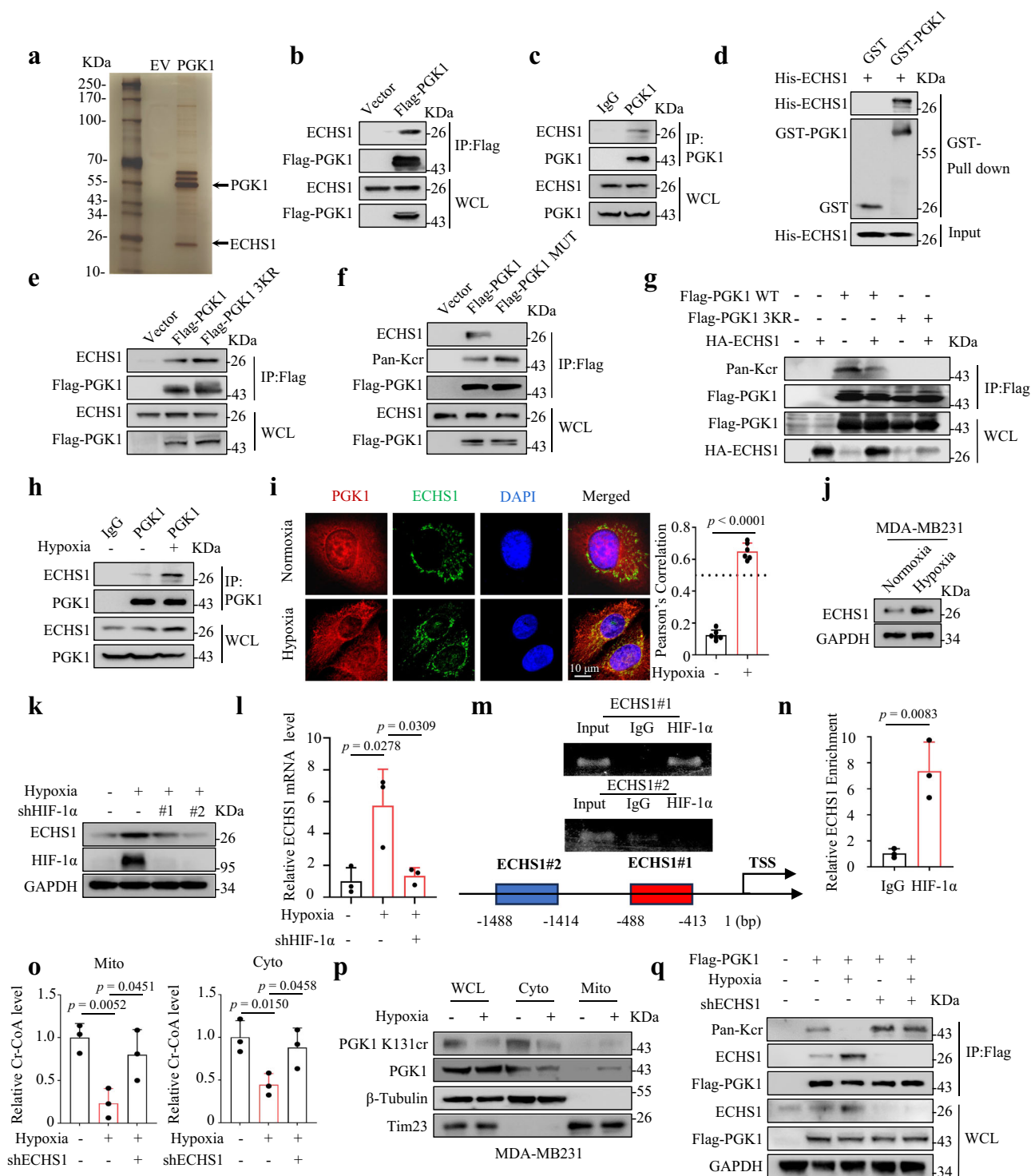


Fig. 2 | PGK1 Kcr at K131, K156, and K220 sites decrease under hypoxia. **a, b** The MS/MS spectrum (**a**) and extracted ion chromatograms from LC-MS/MS analysis (**b**) of the in vivo derived PGK K131cr peptide, the synthetic standard PGK K131cr peptide, and their mixture. The b ion refers to the N-terminal parts of the peptide, and the y ion refers to the C-terminal parts of the peptide. **c** The ratio and *p* value (unpaired two-tailed Student's *t* test) of PGK1 Kcr on different sites under hypoxia versus normoxia. **d** IP assays were performed with anti-Flag M2 beads using HEK293T cells expressing Flag-tagged PGK1 WT, K131R, K156R, K220R, or 3KR, followed by immunoblotting with pan anti-Kcr and anti-Flag antibodies. **e** Sequence alignment of the PGK1 amino acid residues across various species. **f** Dot blot assays were performed to verify the specificity of PGK1 K131cr antibody against PGK1

K131cr, K156cr, and K220cr. **g** IP assays were performed with anti-Flag M2 beads using HEK293T cells expressing Flag-tagged PGK1 K131R, followed by immunoblotting with the specific antibody against PGK1 K131cr. **h** MDA-MB231 cells were cultured under the stimulation of normoxia or hypoxia for 12 h and subjected to IP assays using anti-PGK1 or anti-IgG antibodies, followed by immunoblotting with the specific antibody against PGK1 K131cr. **i** MDA-MB231 cells were incubated with or without 10 mM sodium crotonate (pH 7.4) and subjected to IP assays using the indicated antibodies, followed by immunoblotting with the specific antibody against PGK1 K131cr. **d, f–i** Data were verified in at least three independent experiments. Source data are provided as a Source Data file.



that PGK1 also acted as a protein kinase to regulate cellular metabolism^{33,34}. Hypoxia induces the phosphorylation of PGK1 at Ser203 and subsequently the translocation of PGK1 to mitochondria, where mitochondrial PGK1 phosphorylates PDHK1 at Thr338, which in turn induces the phosphorylation and inactivation of PDH, thereby suppressing mitochondrial pyruvate metabolism and promoting glycolysis³⁴. Consistent with this finding, mimicking PGK1 S203 phosphorylation by mutating Ser203 to Asp (S203D) promoted the phosphorylation of PDH, which was diminished by the depletion of PDHK1 (Supplementary Fig. 7a). In addition, our immunofluorescence results showed that hypoxia promoted the mitochondrial localization of Flag-

PGK1, as well as Flag-PGK1 3KR, suggesting that crotonylation did not affect the mitochondrial translocation of PGK1 induced by hypoxia (Fig. 5b and Supplementary Fig. 7b). To further explore the effects of Kcr on the PGK1-mediated phosphorylation cascade, we used HEK293T cells expressing Flag-PGK1 or Flag-PGK1 3KR to detect the interaction between PGK1 and PDHK1. Co-IP analysis indicated that abolishment of PGK1 Kcr promoted its interaction with PDHK1 (Fig. 5c). Moreover, we deleted endogenous PGK1 in MDA-MB231 cells using CRISPR/Cas9 technology, then rescued PGK1 expression with sgRNA-resistant PGK1 (rPGK1) WT or 3KR. Subsequently, we depleted ECHS1 in both the rPGK1 WT and 3KR cells (Supplementary Fig. 7c). We found

Fig. 3 | ECHS1 mediates the downregulation of PGK1 crotonylation under hypoxia. **a** IP assays were performed using HEK293T cells expressing Flag-tagged PGK1, followed by silver staining. **b** Co-IP assays were performed using HEK293T cells expressing Flag-tagged PGK1. **c** MDA-MB231 cells were subjected to the Co-IP assays using indicated antibodies. **d** GST pull-down assays were performed using GST-tagged PGK1, His-tagged ECHS1 or GST proteins. **e** Co-IP assays were performed using HEK293T cells expressing Flag-tagged PGK1 WT or 3KR. **f** HEK293T cells were transfected with Flag-tagged PGK1 WT or MUT and subjected to IP assays. **g** IP assays were performed using HEK293T cells co-expressing Flag-tagged PGK1 WT or 3KR with HA-tagged ECHS1. **h** MDA-MB231 cells were cultured under normoxia or hypoxia for 12 h and subjected to IP assays. **i** Immunofluorescence assays were performed using MDA-MB231 cells under normoxia or hypoxia for 12 h. Co-localization was quantified using Pearson's correlation coefficients. **j** ECHS1 was detected in MDA-MB231 cells under normoxia or hypoxia for 12 h. **k** ECHS1 was detected in MDA-MB231 cells expressing scramble or

shHIF-1 α under normoxia or hypoxia. **l** ECHS1 mRNA was detected by qPCR in MDA-MB231 cells with or without HIF-1 α depletion under normoxia or hypoxia for 12 h. **m** Agarose-gel-electrophoresis was performed after CUT&Tag assays using HIF-1 α antibody in MDA-MB231 cells. The locations of positive #1 and negative #2 primers are shown. **n** CUT&Tag qPCR assays were performed in MDA-MB231 cells under hypoxia for 12 h using an anti-HIF-1 α antibody. **o** MDA-MB231 cells with or without ECHS1 depletion were cultured under normoxia or hypoxia for 12 h. The levels of crotonyl-CoA in cytosolic and mitochondrial fractions were analyzed by LC-MS/MS. **p** MDA-MB231 cells were cultured under normoxia or hypoxia for 12 h, followed by fractionation assays. **q** HEK293T cells with or without ECHS1 depletion were transfected with Flag-tagged PGK1 and subjected to IP assays. In **i**, **l**, **n**, **o**, data are shown as the mean \pm SD, $n = 3$ (**l**, **n**, **o**) or 6 (**i**) biologically independent samples (unpaired two-tailed Student's t test). All experimental data were verified in at least three independent experiments. Source data are provided as a Source Data file.

that expression of the rPGK1 3KR mutant resulted in upregulated levels of phosphorylated PDHK1 and PDH compared to rPGK1 WT in the presence or absence of ECHS1 (Fig. 5d). rPGK1 WT cells with ECHS1 depletion exhibited reduced levels of phosphorylated PDHK1 and PDH compared to rPGK1 WT cells (Fig. 5d). As expected, rPGK1 3KR mutant promoted the phosphorylation of PDH in the presence of PDHK1 (Fig. 5e). We also found that the interaction between PGK1 and PDHK1 was enhanced under hypoxia, which was reversed by the expression of shRNA targeting ECHS1 (Fig. 5f and Supplementary Fig. 7d). Furthermore, our results showed that hypoxia or PGK1 S203D increased the phosphorylation of PDHK1 depending on the existence of ECHS1 (Fig. 5g and Supplementary Fig. 7e, f). These results suggest that the downregulation of PGK1 Kcr is important for the phosphorylation and activation of PDHK1 by PGK1 in mitochondria.

We then determined whether PGK1 Kcr regulated mitochondrial pyruvate metabolism and glycolysis. Oxygen consumption rate (OCR) and extracellular acidification rate (ECAR) assays were performed using rPGK1 WT and 3KR cells with or without ECHS1 depletion. Our results showed that rPGK1 WT cells with ECHS1 depletion displayed an increase in OCR and a reduction in ECAR in comparison to rPGK1 WT cells. Conversely, rPGK1 3KR cells exhibited decreased OCR and elevated ECAR compared to rPGK1 WT cells, regardless of the presence or absence of ECHS1 (Fig. 5h, i). Additionally, LC-MS analysis of metabolites in rPGK1 WT- or 3KR-rescued MDA-MB231 cells with or without ECHS1 depletion indicated that promoting PGK1 Kcr by ECHS1 depletion was associated with reduced pyruvate and lactate levels, and elevated levels of TCA cycle metabolites and acetyl-CoA. Conversely, abolishing PGK1 Kcr by mutating lysine sites to arginine resulted in the inverse effects (Fig. 5j, k). Hypoxia also led to the decreased conversion of pyruvate to acetyl-CoA, which was restored by the knockdown of ECHS1 (Supplementary Fig. 7g). We also found that rPGK1 3KR expression inhibited ROS production while ECHS1 depletion promoted ROS production (Fig. 5l). Through the manipulation of PGK1 Kcr by ECHS1 knockdown and the introduction of a non-crotonylated PGK1 mimic, our findings indicate that abrogation of PGK1 crotonylation attenuates mitochondrial pyruvate metabolism and promotes lactate production.

Downregulation of PGK1 crotonylation promotes cell proliferation and tumorigenesis

To further explore the effect of PGK1 Kcr on cell proliferation, we constructed MDA-MB231 cells with or without reconstituted expression of rPGK1 WT or 3KR in PGK1-deleted MDA-MB231 cells (Fig. 6a). Colony formation assays performed using these cells showed that reconstituted expression of rPGK1 WT or 3KR restored the reduction of colony numbers associated with PGK1 deletion, with rPGK1 3KR rescuing colony formation to a greater extent than rPGK1 WT (Fig. 6b, c). In addition, the depletion of ECHS1 in rPGK1 WT cells resulted in a significant inhibition of colony formation when compared to their parental cells (Supplementary Fig. 8a, b) We also found that

rescue with rPGK1 3KR promoted cell growth more efficiently than rPGK1 WT cells in the presence or absence of ECHS1 (Fig. 6d and Supplementary Fig. 8c). However, rPGK1 WT cells with ECHS1 depletion exhibited slower cell proliferation compared to those without ECHS1 depletion (Supplementary Fig. 8c). Excessive lactate production by cancer cells is secreted in the extracellular space and induces tumor cell migration^{35,36}. Because we found that abrogation of PGK1 crotonylation promoted lactate production (Fig. 5i, j), we next determined whether PGK1 crotonylation affects tumor cell migration. Transwell migration assays showed that PGK1 deletion suppressed tumor migration, whereas re-expression of rPGK1 WT or 3KR compensated for the deletion effect on tumor cell migration (Fig. 6e, f). Moreover, rPGK1 3KR re-expression promoted tumor cell migration more effectively than rPGK1 WT, regardless of the presence or absence of ECHS1 (Fig. 6e, f and Supplementary Fig. 8d, e). Our results showed that rPGK1 3KR exhibited faster wound healing activity than rPGK1 WT (Fig. 6g, h and Supplementary Fig. 8f, g). Of note, the promotion of PGK1 Kcr through ECHS1 depletion led to impaired transwell migration and wound healing activity (Supplementary Fig. 8d–g). These findings suggest that downregulation of PGK1 crotonylation promotes tumor cell proliferation and migration in vitro.

Next, we ascertained whether PGK1 crotonylation affected tumor growth in vivo. In xenografted nude mice, tumor growth was significantly impaired by deletion of PGK1, which was restored by reconstituted expression of rPGK1 WT or 3KR (Fig. 6i, j and Supplementary Fig. 8h). Notably, rPGK1 3KR re-expression exhibited more apparent tumor-promoting effects than rPGK1 WT (Fig. 6i, j and Supplementary Fig. 8h). Moreover, immunohistochemistry (IHC) assays confirmed that the PGK1 3KR mutant led to the abolishment of Kcr levels (Supplementary Fig. 8i, j). We further investigated the effect of PGK1 Kcr-pPDHK1-pPDH1 axis on tumor growth both in vitro and in vivo by utilizing rPGK1 WT and 3KR cells with or without PDHK1 depletion (Fig. 6k). Our findings demonstrated that the expression of rPGK1 3KR led to enhanced cell growth compared to rPGK1 WT. However, this effect was abrogated by the expression of shRNA targeting PDHK1 (Fig. 6l). Consistently, the mouse xenograft studies showed that mice injected with rPGK1 3KR cells developed larger tumors compared to those injected with rPGK1 WT cells, which was abolished by PDHK1 knockdown (Fig. 6m–o). Taken together, these results indicate that downregulation of PGK1 crotonylation promotes tumorigenesis.

Low PGK1 K131 crotonylation indicates a poor prognosis in breast cancer patients

To further elucidate the role of PGK1 Kcr in breast cancer development, we first analyzed the level of PGK1 K131cr and PGK1 in normal breast cell line MCF10A and different breast cancer cell lines. We found that the downregulation of PGK1 K131cr and upregulation of PGK1 in breast cancer cell lines (Supplementary Fig. 9a). We then also utilized the normal breast tissues from wild-type (FVB) mice and tumor tissues

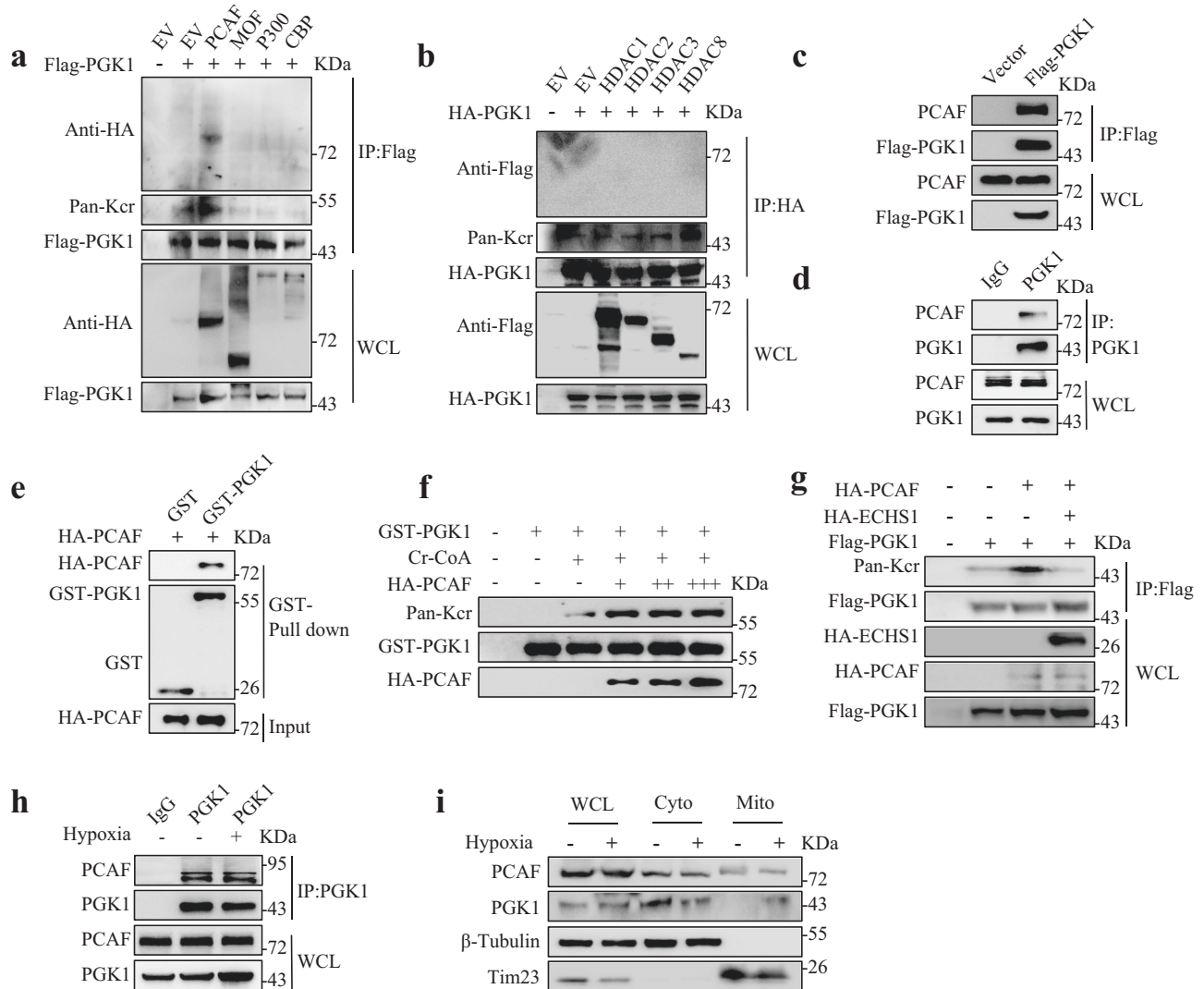
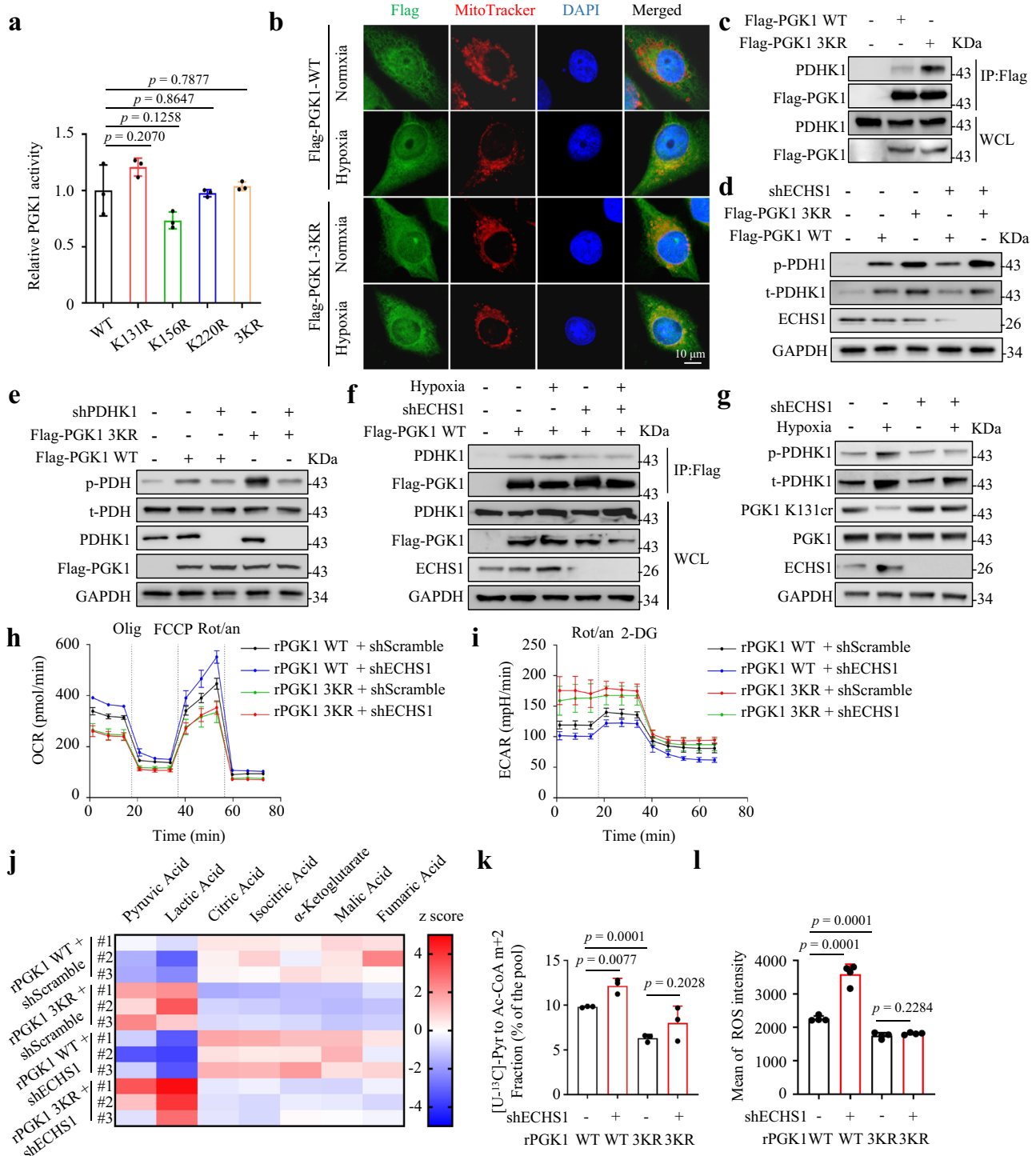


Fig. 4 | PCAF is the crotonyltransferase of PGK1 Kcr. **a** Co-IP assays were performed with anti-Flag M2 beads using HEK293T cells transfected with Flag-tagged PGK1 and HA-tagged HATs, followed by immunoblotting with the indicated antibodies. **b** Co-IP assays were performed with anti-Flag M2 beads using HEK293T cells transfected with HA-tagged PGK1 and Flag-tagged HDACs, followed by immunoblotting with the indicated antibodies. **c** Co-IP assays were performed with anti-Flag M2 beads using HEK293T cells expressing Flag-tagged PGK1, followed by immunoblotting with anti-PCAF and anti-Flag antibodies. **d** MDA-MB231 cells were subjected to IP assays using anti-PGK1 or anti-IgG antibodies, followed by immunoblotting with anti-PCAF and anti-PGK1 antibodies. **e** GST pull-down assays were performed by mixing purified recombinant GST-tagged PGK1 and HA-tagged PCAF proteins, followed by immunoblotting with the indicated antibodies. **f** In vitro

Kcr assays with 5 μ g recombinant GST-tagged PGK1, 50 μ M crotonyl-CoA, and different concentrations of HA-tagged PCAF. The reaction mixtures were analyzed by immunoblotting with the indicated antibodies. **g** IP assays were performed with anti-Flag M2 beads using HEK293T cells expressing the indicated plasmids, followed by immunoblotting with pan anti-Kcr, anti-Flag and anti-HA antibodies. **h** MDA-MB231 cells treated with or without hypoxia were subjected to Co-IP assays using anti-PGK1 or anti-IgG antibodies, followed by immunoblotting with anti-PCAF and anti-PGK1 antibodies. **i** MDA-MB231 cells were cultured under normoxia or hypoxia for 12 h, followed by cell fractionation assays. Immunoblotting was performed to detect the indicated proteins. All experimental data were verified in at least three independent experiments. Source data are provided as a Source Data file.

from the MMTV-PyMT mice with early (week 7) or late (week 18) stages of spontaneous breast cancer to evaluate the significance of PGK1 crotonylation in regulating cancer cells mitochondrial metabolic reprogramming. The IHC assays showed that the expression of PGK1 K131cr was suppressed in breast cancer tissues from MMTV-PyMT mice when compared to normal mouse breast tissues, and late-stage breast cancers exhibited lower levels of PGK1 K131cr in comparison to early-stage cancers (Fig. 7a, b). Moreover, the levels of PGK1, ECHS1, phosphorylated PDHK1, PDHK1, and HIF-1 α showed a gradient increase during this spontaneous mouse breast cancer progression (Fig. 7a, c–g), indicative of a gradual dependence of mitochondrial metabolic reprogramming in breast cancer progression. Furthermore, we analyzed the level of PGK1 K131cr in specimens from six pairs of breast

cancer and adjacent normal breast tissues. We found that PGK1 K131cr expression was notably lower in tumor tissues compared to the level of adjacent normal breast tissue expression (Fig. 7h). Conversely, tumor samples displayed higher levels of ECHS1 and PGK1 expression than adjacent normal breast tissues (Fig. 7h). IHC assays also confirmed that the level of PGK1 K131cr in tumor tissues was lower relative to normal breast tissue samples (Fig. 7i, j). We then compared the duration of 129 breast cancer patients survival with the PGK1 crotonylation levels. A low PGK1 K131cr level was shown to indicate a poor prognosis in breast cancer patients (Fig. 7k). The PGK1 K131cr level was significantly decreased in high-grade breast cancers compared to low-grade breast cancers (Fig. 7l). Moreover, a high lymphocytic infiltration was associated with a low PGK1 K131cr level (Fig. 7l).



Next, we performed IHC assays to determine the expression of ECHS1 in breast cancer and adjacent normal breast tissues. ECHS1 expression was markedly increased in tumor tissues (Fig. 7m and Supplementary Fig. 9b). The PGK1 crotonylation levels were negatively correlated with the level of ECHS1 expression (Supplementary Fig. 9c). In addition, based on data from breast cancer in the cancer genome atlas (TCGA), we found that patients with high levels of ECHS1 had shorter overall survival times (Fig. 7n). Because PGK1 is highly expressed in many types of cancer and is closely associated with poor prognosis in patients with tumors^{37–39}, We then analyzed the RNA-sequencing data of breast cancer in the GEO datasets. Our results showed that tumor samples displayed higher levels of PGK1 expression

compared to adjacent normal breast tissues (Supplementary Fig. 9d). Furthermore, PGK1 expression was positively correlated with immune infiltration of invasive breast cancer patients and poor prognosis (Supplementary Fig. 9e, f). The IHC assays indicated that PGK1 was highly expressed in the tumor samples (Supplementary Fig. 9g, h). Taken together, these data elucidate the role of ECHS1-regulated PGK1 crotonylation in the clinical behavior of human breast cancer.

Discussion

Herein we utilize a quantitative proteomics approach to explore the global crotonylome under normoxia and hypoxia. Among hypoxia-responsive Kcr proteins, PGK1, an enzyme essential for glycolysis, is

Fig. 5 | PGK1 crotonylation is indispensable for coordinating mitochondrial pyruvate metabolism and glycolysis. **a** The enzymatic activity of Flag-tagged PGK1 WT, K131R, K156R, K220R, or 3KR purified from HEK293T cells were measured. **b** MDA-MB231 cells expressing Flag-tagged PGK1 WT or 3KR were stimulated with or without hypoxia for 12 h and stained with anti-Flag antibody and Mito-Tracker. Nuclei were stained with DAPI. **c** Co-IP assays were performed using HEK293T cells transfected with Flag-tagged PGK1 WT or 3KR. **d** PDHK1 and PDH phosphorylation was detected by immunoblotting in PGK1-deleted MDA-MB231 cells expressing sgRNA-resistant PGK1 (rPGK1) WT or 3KR, with or without shRNA targeting ECHS1. **e** PDH phosphorylation was detected by immunoblotting in PGK1-deleted MDA-MB231 cells expressing sgRNA-resistant PGK1 (rPGK1) WT or 3KR, with or without PDHK1 depletion. **f** MDA-MB231 cells with or without ECHS1 depletion were transfected with Flag-tagged PGK1 and cultured under normoxia or hypoxia for 12 h, followed by Co-IP assays. **g** MDA-MB231 cells with or without

ECHS1 depletion were cultured under normoxia or hypoxia for 12 h, followed by immunoblotting with the indicated antibodies. **h, i** The oxygen consumption rate (OCR, **h**) and the extracellular acidification rate (ECAR, **i**) in MDA-MB231 cells with endogenous PGK1 deletion and reconstituted expression of rPGK1 WT or rPGK1 3KR, with or without ECHS1 depletion. **j** Heat map showing the differential metabolites between MDA-MB231/rPGK1 WT cells and MDA-MB231/rPGK1 3KR cells with or without ECHS1 depletion. Each group had 3 biologically independent samples. **k** The relative levels of [$^{13}\text{C}_3$]-Pyruvate derived m + 2 acetyl-CoA in MDA-MB231/rPGK1 WT cells and MDA-MB231/rPGK1 3KR cells with or without ECHS1 depletion. **l** The levels of mitochondrial ROS were measured using a 2',7'-dichlorodihydrofluorescein diacetate (DCFH-DA) probe. **a, h–l** Data are shown as the mean \pm SD, $n = 3$ (**a, j, k**) or 4 (**h, i, l**) biologically independent samples (unpaired two-tailed Student's *t* test). All experimental data were verified in at least two (**j, k**) or three (**a–i, l**) independent experiments. Source data are provided as a Source Data file.

hit. We confirm a significant decrease in PGK1 K131cr, K156cr, and K220cr under hypoxia, which is mediated by upregulation of ECHS1 and the interaction with PGK1 (Supplementary Fig. 9i). Mutations of these PGK1 Kcr sites impede mitochondrial pyruvate metabolism by activating PDHK1 and promote glycolysis independent of its catalytic activity in glycolysis.

Cancer cells undergo metabolic remodeling in response to hypoxia, switching from mitochondrial pyruvate metabolism and oxidative phosphorylation to cytosolic glycolysis and fermentation⁴⁰. A crucial step in this process is downregulation of PGK1 Kcr. Our study has revealed that hypoxia-induced reduction in crotonylation of PGK1 facilitates the interaction between PGK1 and PDHK1. This interaction leads to the activation of PDHK1, which inhibits the function of PDH1 and suppresses mitochondrial pyruvate metabolism. This metabolic alteration could restrict the production of reactive oxygen species at the electron transport chain, which has the potential to induce cell death. Additionally, the decreased transport of pyruvate to mitochondria also mitigates the accumulation of NADH caused by hypoxia in tumors, which promotes cancer cell proliferation. Overall, our findings underscored the significant role of PGK1 crotonylation in regulating the coordination between glycolysis and the TCA cycle, establishing a link between protein Kcr and metabolic reprogramming under hypoxia. Although our study indicates the crotonylation of PGK1 at K131, K156, and K220 sites influences hypoxia-induced metabolic reprogramming, we cannot rule out the possibility that other lysine PTMs occurring at these three sites could also contribute to this process.

Many types of PTMs occur on PGK1 and have crucial roles in regulating physiologic processes. Specifically, S203 phosphorylation of PGK1 mediates translocation to the mitochondria, and thus inhibits pyruvate metabolism³⁴. Phosphorylation of PGK1 Thr243 promotes glycolysis and tumorigenesis⁴¹. Acetylation of PGK1 K388 by NAA10/ARD1 leads to the phosphorylation of Beclin1 at Ser30, which results in VPS34-Beclin1 complex activation to promote autophagy³³. PGK1 can also be acetylated at the K220 and K323 sites. K220 acetylation inhibits the activity of PGK1, whereas K323 acetylation enhances the activity of PGK1^{42,43}. Furthermore, T255 glycosylation of PGK1 promotes PGK1 activity and induces PGK1 translocation into mitochondria⁴⁴. In addition to the above PTMs, lysine Kcr is a PTM that has been recently identified on histones, which is associated with active gene transcription; however, the understanding of Kcr on non-histone proteins and the physiologic functions is limited. Our study provides evidence supporting the significant role of PGK1 Kcr in mitochondrial metabolic reprogramming. We have identified the crotonyltransferase PCAF responsible for PGK1 Kcr in the cytosol; however, our results indicate that it is not responsible for the reduction of PGK1 Kcr under hypoxia. Although no decrotonylase regulating PGK1 crotonylation has been identified, we demonstrate a unique substrate-level regulation of PGK1 Kcr expression that can be

responsive to hypoxia. ECHS1, a hydratase that hydrolyzes crotonyl-CoA, is upregulated under hypoxia by transcription to reduce the intracellular crotonyl-CoA in both cytosol and mitochondria. Moreover, hypoxia induces the translocation of PGK1 from the cytosol to the mitochondria, where ECHS1 interacts with PGK1, thereby further restricting the availability of crotonyl-CoA for PGK1 crotonylation by degrading crotonyl-CoA surrounding PGK1. Our findings in this unique PGK1 Kcr regulation model at the substrate level may facilitate further research on Kcr or PGK1 PTMs. Nevertheless, the crosstalk between the multiple PGK1 PTMs in determining activity and function needs to be further elucidated.

Under hypoxia, PGK1 Kcr is decreased due to the transcriptional upregulation of ECHS1 by HIF-1 α . Upregulation of ECHS1 leads to a reduction in intracellular crotonyl-CoA, thereby impacting the levels of PGK1 Kcr; however, the well-established Warburg effect indicates that oxygenated cancer cells also ferment a large amount of glucose-to-lactate instead of oxidizing glucose in mitochondrial respiration²¹. Given that breast cancer tissue exhibits a low level of PGK1 K131cr compared to the para-carcinoma tissue, our research may provide a molecular mechanism underlying the Warburg effect. PGK1 Kcr might be regulated by other oncogenes than HIF-1 α under normoxia. In such a context, the significance of PGK1 Kcr and ECHS1, as well as the identification of related signaling pathways involved in this regulation, warrant further exploration.

In summary, our finding that PGK1 Kcr functions as a regulatory signal in coordinating glycolysis and the TCA cycle provides insight into the connection between PTMs and metabolic reprogramming. Our results demonstrate that the ECHS1-mediated decrease in PGK1 Kcr plays an important role in the metabolic remodeling of tumor cells to survive the hypoxic microenvironment. Moreover, our results illustrate that breast cancer tissues exhibit lower levels of PGK1 K131cr and higher levels of ECHS1 compared to adjacent normal breast tissues, which can predict a poor prognosis in breast cancer patients. Therefore, PGK1 Kcr could be a promising candidate for the diagnosis and treatment of breast cancer.

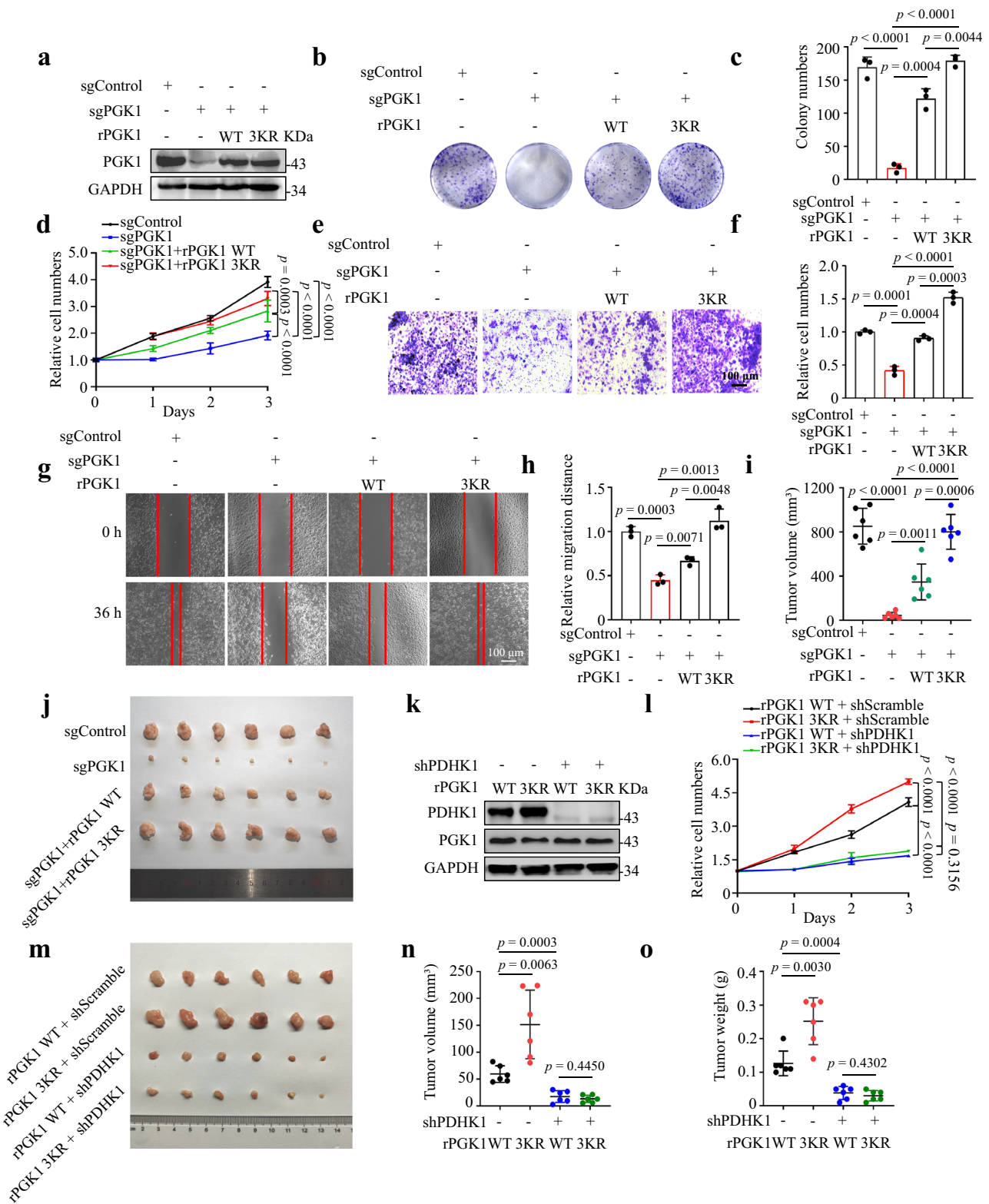
Methods

Study approval

The research performed in this study complies with all relevant ethical regulations. All animal experiments were approved by the Capital Medical University Institutional Animal Care and Use Committee (IACUC) or by the Westlake University IACUC.

Antibodies and reagents

The antibodies used in this study were listed as follows: anti-PGK1 (Proteintech, 17811-1-AP, 1:2000 dilution), anti-rPGK1 (Santa Cruz, sc-130335, 1:1000 dilution), anti-Crotonyllysine (PTM BIO, PTM-501, 1:500 dilution), anti-Acetyllysine (PTM BIO, PTM-105, 1:500 dilution), anti-ECHS1 (Proteintech, 11305-1-AP, 1:500 dilution), anti-GAPDH



(Proteintech, 60004-1-Ig, 1:1000 dilution), anti-VHL (Proteintech, 24756-1-AP, 1:500 dilution), anti-HIF-1 alpha (Proteintech, 20960-1-AP, 1:1000 dilution), anti-PCAF (Santa Cruz, sc-13124, 1:1000 dilution), anti-PDHK1 (Proteintech, 18262-1-AP, 1:2000 dilution), anti-phospho-PDHK1 (Thr338) (Signalway, 11596, 1:500 dilution), anti-Flag M2 (Sigma-Aldrich, F1804, 1:5000 dilution), anti-GST (Proteintech, 66001-2-Ig, 1:5000 dilution), anti-His (Proteintech, 66005-1-Ig, 1:5000 dilution), anti-HA (Proteintech, 51064-2-AP, 1:3000 dilution), anti-mouse

IgG (H+L)/HRP (Jackson, 115-035-003, 1:10000 dilution), anti-rabbit IgG (H+L)/HRP (Jackson, 111-035-003, 1:10000 dilution), anti-rabbit IgG (H+L)/FITC (ZSGB-Bio, ZF-0311, 1:200 dilution), anti-rabbit IgG (H+L)/TRITC (ZSGB-Bio, ZF-0316, 1:200 dilution), anti-mouse IgG (H+L)/FITC (ZSGB-Bio, ZF-0312, 1:200 dilution), anti-mouse IgG (H+L)/TRITC (ZSGB-Bio, ZF-0313, 1:200 dilution). Rabbit polyclonal anti-crotonyl-PGK1 (K131) was custom-made by PTM to detect PGK1 K131 site-specific crotonylation levels.

Fig. 6 | Downregulation of PGK1 crotonylation promotes cell proliferation and tumorigenesis. **a** Reconstituted expression of the rPGK1 WT or 3KR proteins was performed in endogenous PGK1-deleted MDA-MB231 cells. The expression of PGK1 was detected by immunoblotting. **b, c** The colony formation of MDA-MB231 cells with or without PGK1 deletion and with or without reconstituted expression of rPGK1 WT or 3KR. The images (**b**) and counted colony numbers (**c**) of indicated groups were shown. **d** Cell proliferation of MDA-MB231 cells with or without PGK1 deletion and with or without reconstituted expression of rPGK1 WT or 3KR. **e, f** Cell invasion ability of MDA-MB231 cells with or without PGK1 deletion and with or without reconstituted expression of rPGK1 WT or 3KR. The images (**e**) and counted invasive cell numbers (**f**) of indicated groups were shown. **g, h** Cell migration of MDA-MB231 cells with or without PGK1 deletion and with or without reconstituted expression of rPGK1 WT or 3KR. The images (**g**) and relative migration distance (**h**),

were shown. **i, j** MDA-MB231 cells with or without PGK1 deletion and with or without reconstituted expression of rPGK1 WT or 3KR were subcutaneously injected into nude mice. Tumor volume (**i**) and tumor formation (**j**) were measured. **k** PDHK1 and PGK1 expression in MDA-MB231/rPGK1 WT cells, MDA-MB231/rPGK1 3KR cells with or without PDHK1 depletion. **l** Cell proliferation of MDA-MB231/rPGK1 WT cells, MDA-MB231/rPGK1 3KR cells with or without PDHK1 depletion. **m–o** MDA-MB231/rPGK1 WT cells, MDA-MB231/rPGK1 3KR cells with or without PDHK1 depletion were subcutaneously injected into nude mice. Tumor formation (**m**), tumor volume (**n**), and tumor weight (**o**) were measured. In **c, d, f, h, i, l, n, o**, data are shown as the mean \pm SD, $n = 3$ (**c, d, f, h, l**) or 6 (**i, n, o**) biologically independent samples. *P* values were obtained using unpaired two-tailed Student's *t* test (**c, f, h, i, n, o**) or two-way ANOVA with Sidak test (**d, l**). Data were verified in at least two (**i, j, m–o**) or three (**a–h, k, l**) independent experiments. Source data are provided as a Source Data file.

The reagents used in this study were listed as follows: Crotonic acid (Sigma-Aldrich, 113018), Sodium acetate (Sigma-Aldrich, S2889), Crotonoyl coenzyme A trilithium salt (Sigma-Aldrich, 28007), Acetyl-coenzyme A trisodium salt (Sigma-Aldrich, 2056), Glyceraldehyde 3-phosphate (Sigma-Aldrich, 39705), β -NAD (Sigma-Aldrich, N8285), ADP (Sigma-Aldrich, A2754), GAPDH (Sigma-Aldrich, G5262), $MgCl_2$ (Sigma-Aldrich, M8266), Ammonium acetate (Solarbio, A7030), Trichloroacetic acid (Sigma-Aldrich, T6399), Protease inhibitor cocktail (Sigma-Aldrich, 539134), H2DCFDA (MCE, HY-D0940), Mito-tracker (Invitrogen, 22425), Glutathione reduced (Solarbio, G8180), DMEM powder (Caisson, DMP52-10LT), Opti-MEM (Gibco, 31985-070), Puromycin (Gibco, A1113803), Blastidicin (Gibco, A1113903), ECHS1 Fusion protein (Proteintech, Ag16775).

Cell lines and plasmids

MDA-MB231 (ATCC, HTB-26), MDA-MB468 (ATCC, HTB-132), T47D (ATCC, HTB-133), HCC1806 (ATCC, CRL-2335), MCF 10 A (ATCC, CRL-10317) and HEK293T (ATCC, CRL-3216) cells were purchased from the American Type Culture Collection. MDA-MB231, MDA-MB468, T47D, and HEK293T cells were maintained in Dulbecco's modified Eagle medium (DMEM, Gibco, C11995500BT) and HCC1806 in RPMI-1640 medium (Gibco, C11875500BT) with 10% fetal bovine serum (FBS, Gibco, 10099141 C) and 1% Penicillin-Streptomycin (Biosharp, BL505A). MCF10A was maintained in a specific commercial medium (Procell, CM-0525). To induce hypoxia, cells were cultured in 0.5% oxygen condition. All the cell lines were tested for mycoplasma contamination, and no commonly misidentified cell lines were used. Transfection was performed using Lipo8000™ transfection reagent (Beyotime, C0533).

The cDNAs of human PGK1 WT and mutants, PCAF and ECHS1 were amplified by PCR. For overexpression, PGK1 WT and mutants, PCAF, ECHS1 and SIRT2, 3 were cloned into vector pCDHO-CMV-3 \times Flag or pCMV-3 \times HA. Flag-HDAC1, 2, 3, 8 were donated by Dr. Jianyuan Luo Lab (Peking University). For protein purification, the PGK1 was cloned into pGEX-4T-1 vector. The oligonucleotides of human PGK1, ECHS1, VHL, and HIF-1 α were synthesized from RuiBiotech (Beijing, China). For gene knockout, PGK1 and VHL oligonucleotides were cloned into vector LentiCRISPRv2. For gene depletion, ECHS1 and HIF-1 α oligonucleotides were cloned into vector pLKO.1. The sequences of oligonucleotides used in this study are listed as follows: ECHS1-sh#1: GCTTGCCATGATGTGTGATAT, ECHS1-sh#2: CCTGAGTTCCAG-GACTGTTA, PGK1-sg#1: ACCTCTGGTTGTTTGTATC, PGK1-sg#2: CAGGGATGTTCTGTTCTTGA, VHL-sg#1: CGCGCGTGTGCTGCCGTA, VHL-sg#2: TGACTAGGCTCCGACAACC, HIF-1 α -sh#1: CGGCGAAGTAAAGAATCTGAA, HIF-1 α -sh#2: CCGCTGGAGACACAATCATAT.

Real-time RT-PCR assays

The total RNA was extracted from MDA-MB231 cells cultured under normoxia or hypoxia for 12 h using an RNA-quick purification kit (EC Science, RN001). Afterward, the total RNA was reverse transcribed into

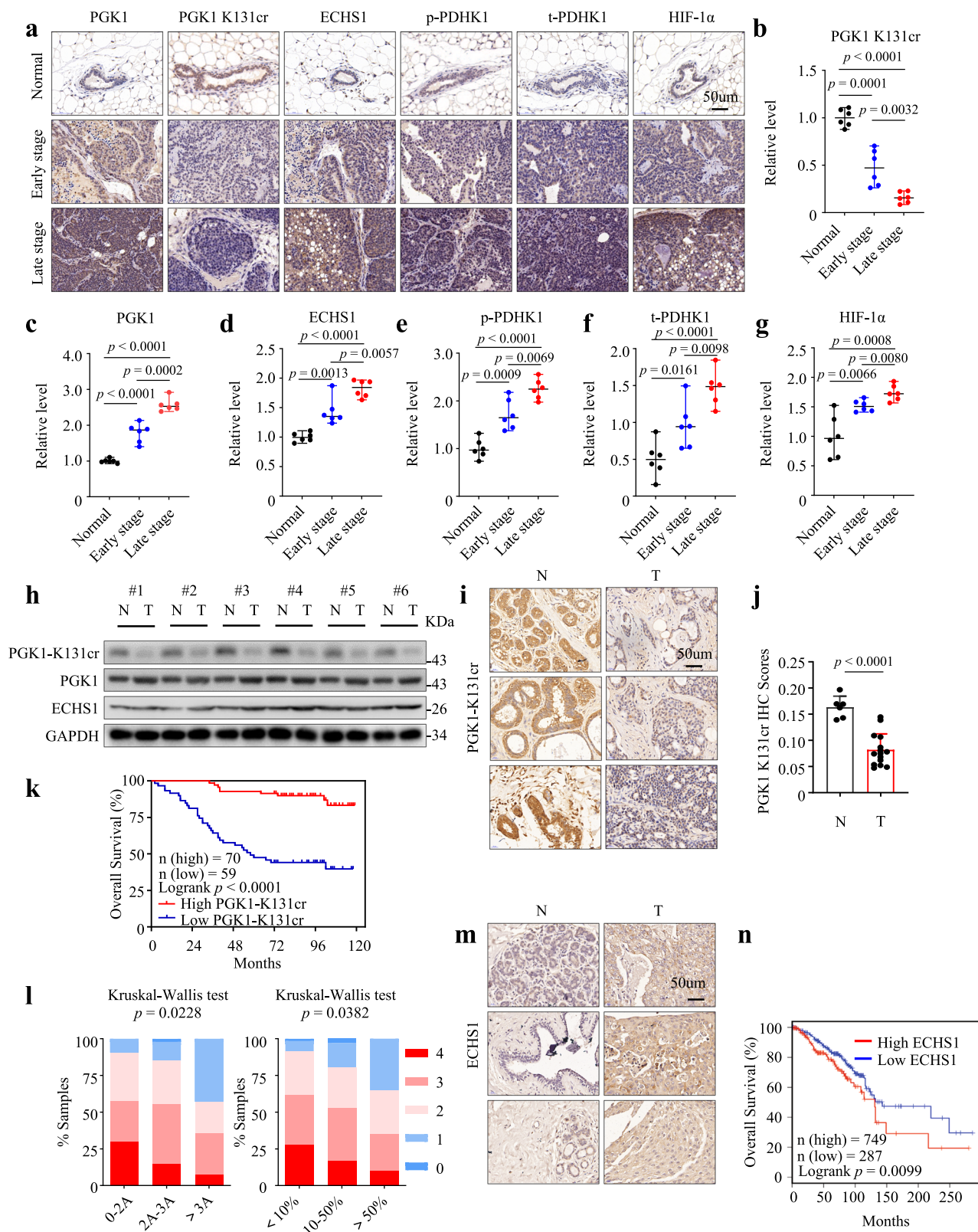
cDNA using HiScript II 1st strand cDNA synthesis kit (Vazyme, R223-01). Quantitative real-time PCR was performed using SYBR qPCR master mix (Vazyme, Q311-02) and Applied Biosystems 7500 Fast instrument (Life Technologies). The primers used for the target genes are shown as follows: ECHS1-F: CCAGGACTGTACTCCAGCAAGTTC; ECHS1-R: TGGTGAAGACGCCAGTGGG; GAPDH-F: GCACCGTCAAGGCTGAGAAC; GAPDH-R: TGGTGAAGACGCCAGTGGG. Otherwise, a qualitative analysis of HIF-1 α targeted ECHS1 promoter was performed using SYBER qPCR master mix (Vazyme, Q311-02) and Applied Biosystems 7500 Fast instrument (Life Technologies) followed by Cut&tag assay kit (Vazyme, TD903). The sequences of ECHS1 promoters are shown as follows: ECHS1 promoter #1-F: AATGTGGCGTTCAG, ECHS1 promoter #1-R: TGTAGCAGCGGAC, ECHS1 promoter #2-F: ATCGTTTACTAAAGG, ECHS1 promoter #2-R: GGGTAAAAATGAAGA.

Quantitative crotonylome analysis

MDA-MB231 cells were cultured in DMEM supplemented with 10% dialyzed FBS in 100 mm dishes at 80% confluence. The experiment consisted of two groups: a normoxic group and a hypoxic group, with $n = 3$ biologically independent samples in each group. After 12 h hypoxia or normoxia treatment, the cells were harvested and washed twice with ice-cold phosphate-buffered saline (PBS) before they were sonicated three times in lysis buffer (8 M urea, 1% protease inhibitor cocktail, 3 μ M TSA, and 50 mM NAM). The supernatant was collected by centrifugation at 12,000 $\times g$ for 10 min at 4 $^{\circ}C$, and the protein concentration was estimated by the Enhanced BCA protein assay kit (Beyotime, P0009). After trypsin digestion, peptides were collected and processed for TMT labeling. One unit of TMT reagent was briefly thawed and reconstituted in acetonitrile. The peptide mixtures were then incubated for 2 h at room temperature and pooled and desalted. The pre-washed antibody beads (PTM Biolabs, Hangzhou) were incubated with tryptic peptides in NETN buffer (50 mM Tris-HCl, pH 8.0, 100 mM NaCl, 1 mM EDTA, 0.5% NP-40) to enrich peptides with lysine crotonylation (Kcr). The beads were washed four times with NETN buffer and twice with H_2O . The peptides were eluted from the beads, desalted with C18 ZipTips (Millipore), and analyzed by LC-MS/MS according to the manufacturer's instructions. Data analysis was processed by the Maxquant search engine (v.1.5.2.8) and searched against the human UniProt database concatenated with the reverse decoy database. The false discovery rate was adjusted to <1% and the minimum score for modified peptides was set to >40.

Generation and purification of the PGK1 K131cr/156cr antibody

Based on the sequence information, two modified and one unmodified polypeptides corresponding to each site were synthesized and conjugated with KLH. After being diluted with physiological saline and mixed 1:1 with the corresponding adjuvant, the immunogen was injected into six New Zealand rabbits four times in 5 weeks. On the 45th day, 30 mL of whole blood was collected and centrifuged to obtain the supernatant for serum screening. Subsequent collections of 20 mL of



whole blood were performed on the 50th, 65th, and 70th days. Positive serum samples were purified using a protein A column and eluted with 150 mM glycine buffer. The crude IgG obtained was loaded onto an equilibrated immunogen affinity chromatography column to specifically enrich the target antibody. Further purification was carried out using an unmodified affinity chromatography column to remove non-specific antibody components. The resulting effluent was directly

collected, and 10% glycerol was added to the purified antibody before it was aliquoted and stored at -20°C .

HPLC-MS/MS analysis

The tryptic peptides were loaded onto a homemade reversed-phase analytical column (25 cm length \times 100 μm i.d.) connected to an EASY-nLC 1200 UPLC system (Thermo Fisher Scientific). The peptides were

Fig. 7 | Low K131 crotonylation of PGK1 indicates a poor prognosis in breast cancer patients. **a–g** IHC staining (**a**) and the quantitative results (**b–g**) of PGK1 K131cr, PGK1, ECHS1, p-PDHK1, t-PDHK1 and HIF-1 α expression in the normal breast tissues from wild-type (FVB) mice and tumor tissues from the MMTV-PyMT mice with early (week 7) or late (week 18) stages of spontaneous breast cancer. Data are shown as the mean \pm SD, $n = 6$ biologically independent samples (unpaired two-tailed Student's t test). **h** Expression of PGK1 K131cr, PGK1 and ECHS1 were detected by immunoblotting in samples from the adjacent normal breast tissues (N) and breast tumor tissues (T) using the indicated antibodies. **i, j** IHC staining (**i**) and the quantitative results (**j**) of PGK1 K131cr expression in samples from adjacent normal breast tissues and breast tumor tissues. Data are shown as the mean \pm SD, n (N) = 6

and n (T) = 15 biologically independent samples (unpaired two-tailed Student's t test). **k** Kaplan–Meier survival curve showing the overall survival of breast cancer patients according to the levels of PGK1 K131cr expression detected by IHC staining. n (high, 3–4 staining degree) = 70, n (low, 0–2 staining degree) = 59 (log-rank). **l** PGK1 K131cr expression in breast tumor tissues from patients at different grades (left) or from patients with different lymph node-positive rates (right). **m** IHC staining of ECHS1 in samples from adjacent normal breast and breast tumor tissues. **n** Kaplan–Meier survival curve depicting the overall survival of breast cancer patients based on ECHS1 expression in the TCGA cohort. n (high) = 749, n (low) = 287 (log-rank). Source data are provided as a Source Data file.

separated and eluted with a gradient of 10–80% buffer B (0.1% formic acid, 90% acetonitrile/in water) in buffer A (0.1% formic acid, 2% acetonitrile/in water) at a flow rate of 500 nl/min over 60 min. The separated peptides were analyzed in Orbitrap Exploris 480 with a nano-electrospray ion source. The electrospray voltage was 2300 V. Precursors and fragments were analyzed with the Orbitrap detector. The full MS scan resolution was set to 60000 for a scan range of 400–1200 m/z . The MS/MS scan was fixed first mass as 110 m/z at a resolution of 15,000 with the TurboTMT set as off. Up to 10 most abundant precursors were then selected for further MS/MS analyses with 30 s dynamic exclusion. The HCD fragmentation was performed at a normalized collision energy (NCE) of 27%. The automatic gain control (AGC) target was set at 100%, with an intensity threshold of 20,000 ions/s and a maximum injection time of 100 ms.

Mass spectrometry analysis of crotonyl-CoA

The crotonyl-CoA extraction assays were performed following the procedure described previously¹⁵. Briefly, MDA-MB231 cells cultured in four 100 mm dishes were washed twice with ice-cold PBS, collected by gently scraping and centrifuged at 1000 $\times g$ for 5 min at 4 $^{\circ}C$. The cell pellets were resuspended in 1 ml of ice-cold extraction solution (10% trichloroacetic acid) and sonicated for 30 s at a rate of 1 pulse per second, followed by centrifugation at 15,000 $\times g$ for 5 min at 4 $^{\circ}C$ to remove protein. The supernatants were then loaded onto the Oasis HLB Cartridge SPE columns (Waters, 186000383), which were conditioned with 1 ml of methanol and equilibrated with 1 ml of water. After washing the columns with 1 ml of water, acyl-CoAs were eluted into new tubes by applying three subsequent applications of 0.5 ml of elution solution (25 mM ammonium acetate/ methanol). The samples were dried under nitrogen gas and stored at $-80^{\circ}C$ until analysis.

The analysis was conducted on a 6500plus QTrap mass spectrometer (AB SCIEX, USA) coupled with the ACQUITY UPLC H-Class system (Waters, USA). Mobile phase A is 5 mM ammonium bicarbonate in HPLC-grade water and mobile phase B is 100% HPLC-grade methanol. A linear gradient is: 0 min, 0% B; 1.5 min, 0% B; 6 min, 95% B; 7.4 min, 95% B; 7.5 min, 0% B; and 10 min, 0% B. Flow rate was 0.3 mL/min. The column chamber and sample tray were held at 40 $^{\circ}C$ and 10 $^{\circ}C$, respectively. Data were acquired in multiple reaction monitor (MRM) modes for CrCoA with transitions of 836.0/329.2 in positive mode. The ion transitions were optimized using chemical standards. The nebulizer gas (Gas1), heater gas (Gas2), and curtain gas were set at 55, 55, and 30 psi, respectively. The ion spray voltage was 5 kV. The optimal probe temperature was 500 $^{\circ}C$ and the column oven temperature was 35 $^{\circ}C$. The SCIEX OS 1.6 software was applied for metabolite identification and peak integration.

Targeted metabolites

MDA-MB231 cells were grown in 100 mm dishes until 80% confluent. The medium was changed and replaced with DMEM lacking glucose, glutamine and pyruvate, and supplemented with 10 mM glucose, 1 mM glutamine, and 10% dialyzed FBS for 8 h. Cells were washed three times with 1 ml of ice-cold PBS and then the polar metabolites were extracted in 1.5 ml of 80% methanol (pre-chilled to $-80^{\circ}C$). After centrifugation

at 14,000 $\times g$ for 20 min at 4 $^{\circ}C$, the supernatants were dried under nitrogen gas and stored at $-80^{\circ}C$ until analysis.

The analysis was conducted on TSQ Quantiva (Thermo, CA) with C18-based reverse-phase chromatography. Mobile phase A is 10 mM tributylamine and 15 mM acetate in HPLC-grade water and mobile phase B is 100% HPLC-grade methanol. This analysis was focused on glycolysis and the TCA cycle. A 25 min gradient from 5% to 90% buffer B was applied. Data were obtained using the positive/negative switching mode. Spray voltages used for positive and negative modes were set at 3.5 kV and 2.5 kV, respectively. The resolutions for Q1 and Q3 were both 0.7FWHM. The source mass spectrometer parameters are shown as follows: capillary temperature 320 $^{\circ}C$, heater temperature 300 $^{\circ}C$, sheath gas flow rate 35, and auxiliary gas flow rate 10. Tracefinder 3.2(Thermo) search with a home-built database containing about 300 compounds was used for metabolite identification.

Metabolite profiling and isotope tracing

MDA-MB231 cells were grown in 100 mm dishes until 80% confluent. The medium was changed and replaced with DMEM lacking glucose, glutamine, and pyruvate, and supplemented with 10 mM glucose, 1 mM glutamine, 1 mM [$U-^{13}C_3$]-pyruvate and 10% dialyzed FBS. After 12 h of culture, cells were washed three times with 1 ml of ice-cold PBS and then the polar metabolites were extracted in 1.5 ml of 80% methanol (pre-chilled to $-80^{\circ}C$). After centrifugation at 14,000 $\times g$ for 20 min at 4 $^{\circ}C$, the supernatants were dried under nitrogen gas and stored at $-80^{\circ}C$ until analysis.

The analysis was performed on a TSQ Quantiva triple quadrupole mass spectrometer coupled to a Dionex Ulti-Mate 3000 UPLC system (Thermo Fisher Scientific). Samples were resuspended in 50 μL 80% methanol, with 1 μL of the suspension added into a Synergi Hydro-RP 100 A 2.1 \times 100 mm column (Phenomenex) for metabolite separation at 35 $^{\circ}C$. Mobile phase A was 10 mM tributylamine in aqueous with pH = 5 and mobile phase B was 100% methanol. The chromatographic gradient was set for mobile phase B as follows: 0–3.5 min: 1% B; 3.5–22 min: from 1% to 70% B; 22–23 min: from 70% to 90% B; 23–25 min: 90% B; 25–30 min: 1% B. Data were acquired using the positive/negative switching method with spray voltages of 3.5 and 2.5 kV, respectively. Q1 and Q3 resolution were set at 0.7, and cycle time was 1 s. Quantitation of Ac-CoA was performed with Tracefinder (Thermo Fisher Scientific). Retention times and ion transitions were validated according to chemical standards. Ion pairs were obtained based on precursors' and fragments' chemical structures. The abundance of each mass isotopomer of Ac-CoA was then mathematically corrected to eliminate natural abundance isotopes and finally converted into a percentage of the total pool.

Glucose uptake and lactate excretion

Glucose and lactate concentrations in the medium were measured using the M-100 Automatic Biosensors Analyzer (Shenzhen SiemenTechnology Co., Ltd) according to the manufacturer's instructions. The glucose consumption and lactate production were normalized by cell numbers.

ECAR and OCR

OCR and ECAR were determined using the Agilent Seahorse XF Analyzer following the manufacturer's protocol. For OCR measurement, 1×10^5 cells were plated in Seahorse XF24 assay plates and incubated in XF base medium (Agilent, 102353-100) overnight. The mitochondrial function was measured using the Agilent Seahorse XF cell mito stress test kit (Agilent, 103015-100). OCR was determined following the sequential addition of oligomycin (2.5 μ M), FCCP (2 μ M), and rotenone (0.5 μ M) plus antimycin A (0.5 μ M) to the system. For ECAR measurement, 3×10^4 cells were plated in Seahorse XF96 assay plates and incubated overnight. Agilent seahorse XFp glycolytic rate assay kit (Agilent, 103344-100) was used to measure the glycolytic rate. ECAR was determined following the sequential addition of rotenone (0.5 μ M) plus antimycin A (0.5 μ M), and 2-DG (50 mM) to the system. The cell number was used for data normalization.

Immunoprecipitation and immunoblotting

The immunoprecipitation assays were performed following the procedure described previously with modifications⁴⁵. Cells were rinsed twice with ice-cold PBS and collected into PBS by scraping. After centrifugation at $500 \times g$ for 5 min at 4 °C, the cell pellets were resuspended with IP buffer (50 mM Tris-HCl, pH 7.5, 150 mM NaCl, 1 mM EDTA, 1% Nonidet P-40, 1% protease inhibitor cocktail) and lysed at 4 °C with constant rotation for 2 h. The cell lysates were centrifuged at $16,000 \times g$ for 15 min at 4 °C and then 5% of the supernatants were collected as whole-cell lysate (WCL) samples. The remaining supernatants were incubated with antibody-coated beads or FLAG-M2 affinity gel (Sigma, A2220) or Anti-HA magnetic beads (Sigma-Aldrich, SAE0197), at 4 °C with constant rotation for 4 h or overnight. The beads were then washed three times with ice-cold IP buffer. The precipitated proteins were eluted from the FLAG-M2 affinity gel using 400 μ g/ml Flag peptides (MCE, HY-P0223), 400 μ g/ml HA peptide (Beyotime, P9808), or directly denatured by heating at 95 °C for 10 min. The immunoprecipitated and WCL samples were separated by SDS-PAGE, then transferred onto a polyvinylidene fluoride (PVDF, Millipore, IPVH00010) membrane, followed by immunoblotting with the indicated primary antibodies and secondary antibodies.

Immunofluorescence assays

MDA-MB231 cells growing on the surface of coverslips were fixed in cold methanol at -20 °C for 10 min and then washed three times with PBS. Then cells were blocked with 1% bovine serum albumin (BSA) in PBS for 30 min, followed by incubation with appropriate primary antibodies at 4 °C overnight and the secondary antibody for 1 h at room temperature. The DNA was stained with DAPI. Images were taken using a confocal laser-scanning microscope (LSM880, Carl Zeiss) with a $\times 63$ oil-immersion objective with numerical aperture (NA) of 1.4 (Plan-Apochromat $\times 63/1.4$ Oil DIC M27, Carl Zeiss).

Tissue microarray and IHC

Breast cancer tissue microarrays of patients (HBreD020PG01, HBreD131Su08, HBreD055CD01) were purchased from Shanghai Outdo Biotech Co., Ltd. IHC staining was performed following the standard procedure. All the slides were dewaxed in xylene, rehydrated in graded ethanol, and then subjected to heat-induced antigen retrieval by heating in a microwave using a citrate-based antigen retrieval solution. After immersing in 0.3% H₂O₂ for 10 min to suppress endogenous peroxidase activity, the slides were sequentially blocked with 5% BSA/PBS for 30 min at room temperature, incubated with the indicated primary antibodies at 4 °C overnight, and incubated with HRP-conjugated secondary antibody for 1 h at room temperature. For color development, the slides were incubated with 3, 3'-diaminobenzidine (ZSGB-Bio, ZLI-9017). The tissue microarrays were scanned

by Panoramic scan (3DHISTECH Ltd.). The protein expression level was evaluated by staining intensity using Aperio Imagescope software (Leica) and images of representative fields were obtained using the Caseviewer (3DHISTECH Ltd.).

Protein purification and in vitro pull-down assays

pGEX-4T-1 construct of GST-fusion PGK1 were expressed in *Escherichia coli* BL21 cells. Protein expression was induced by the addition of 0.5 mM isopropyl IPTG (b-D-1-thiogalactopyranoside, Solarbio, I8070) at 18 °C for 16 h. Cells were harvested and resuspended in PBS. After sonication and centrifugation, the supernatant was loaded onto a GSTrap column (Cytiva, 17528201) equilibrated with PBS. After being washed with 10 column volumes of PBS, the bound proteins were eluted using 10 mM glutathione (Solarbio, G8180) in PBS. For in vitro pull-down assays, 5 μ g recombinant GST-tagged PGK1 or recombinant GST were incubated with glutathione resin in PBS at 4 °C with constant rotation for 1 h. The protein-bound resin was then washed with ice-cold PBS before incubating with 2.5 μ g His-tagged ECHS1 or PCAF at 4 °C with constant rotation for 1 h. After being washed three times with PBS, the resin was denatured by heating at 95 °C for 10 min and analyzed using immunoblotting.

In vitro crotonylation assays

For in vitro crotonylation assays, 5 μ g recombinant GST-tagged PGK1 were incubated with 100 μ M crotonyl-CoA, and 0.5, 1, or 2.5 μ g recombinant His-tagged PCAF at 30 °C for 1 h in buffer A (50 mM Tris, pH 8.0, 10% glycerol, 1 mM DTT, 0.2 mM PMSF). The mixture was denatured by heating at 95 °C for 10 min and analyzed by immunoblotting.

In vitro enzyme activity assay

Flag-tagged PGK1 WT, K131R, K156R, K220R, or 3KR were immunoprecipitated from HEK293T cells. To evaluate the PGK1-catalyzed reaction of 3-PG production, the reactions were conducted in buffer containing 5 mM KH₂PO₄ (pH 7.0), 8 mM MgCl₂, 1 mM glyceraldehyde 3-phosphate, 0.3 mM β -NAD, 0.2 mM ADP, 100 mM glycine and GAPDH (5 ng/ μ L) at room temperature. The change in absorbance at 340 nm owing to the increase of NADH was measured using TriStar² LB 942 multimode microplate reader (Berthold Technologies).

Colony formation assays

For colony formation assay, 1000 cells per well were seeded into six-well plates in triplicates. After 2 weeks, colonies were fixed with methanol and stained with 0.5% crystal violet for 20 min.

Migration assays by transwell

The melted matrigel (BD-Biosciences, 356234) was diluted in the cold serum-free medium and mixed thoroughly. Then the diluted matrigel matrix was added to the upper chamber of each transwell (BD-Biosciences, 356234) insert and incubated at 37 °C for 3 h. 2.0×10^5 MDA-MB231 cells were resuspended in 0.5 mL serum-free medium and 200 μ L of the cell suspension was seeded into the upper chamber. The chamber was transferred in a well containing 500 μ L medium with 10% FBS. After 24 h, the chamber was fixed with 4% paraformaldehyde for 30 min, dyed with 0.1% crystal violet for 10 min and then counted.

Migration assays by wound healing

MDA-MB231 cells were plated in six-well plates in triplicates until 90% confluent and then wounded with RNase-free pipette tips and washed with PBS to remove any floating cells. Photos were captured at 0 h, 12 h, 24 h, or 36 h after treatment. Wound healing was evaluated by measuring the remaining distances between the wound edges at the endpoint.

Tumor xenografts in nude mice model and spontaneous tumor model

Female BALB/c nude mice (6 weeks old) were purchased from Beijing Vital River Laboratory Animal Technology Co., Ltd. Female FVB/N-Tg(MMTVPyVT)634Mul/J mice were purchased from the Jackson Laboratory. Female FVB mice were purchased from Shanghai SLAC Laboratory Animal Company. All the procedures using animals were approved by the Capital Medical University IACUC or by the Westlake University IACUC. The mice were housed in a pathogen-free animal barrier facility. For the spontaneous tumor model, the purchased FVB/N-Tg(MMTVPyVT)634Mul/J mice were maintained until sacrificed at 7 and 18 weeks old, and the tumor tissues were harvested. For xenografts model, briefly, 1×10^6 MDA-MB231 cells (stably expressing control Cas9, sgPGK1, rescued with rPGK1 WT or 3KR; rPGK1 WT, rPGK1 3KR with or without PDHK1 depletion) were subcutaneously injected into mice. All of the tumors were harvested and weighed at the end of the experiments. The experiment complied with the ethical guideline that subcutaneous tumor diameter should not exceed 15 mm and the tumor weight below 10% of the mouse body weight ($<2000 \text{ mm}^3$).

Quantification and statistical analysis

The results of all the experiments were generated from at least three biologically independent samples unless noted otherwise in the figure legend. The experiments were repeated at least twice independently with similar results. All the data represent the mean \pm SD. The statistical analyses were conducted using GraphPad PRISM 9.0.2 software. Statistical significance was typically determined using unpaired two-tailed Student's *t* test or two-way analysis of variance with the Sidak test. Differences in overall survival were determined by the Log-rank test.

Reporting summary

Further information on research design is available in the Nature Portfolio Reporting Summary linked to this article.

Data availability

The publicly available data used in this study are available in the GEO database under accession code [GSE22820](#), [GSE26304](#) and Gene Expression Profiling Interactive Analysis⁴⁶. The mass spectrometry proteomics data generated in this study have been deposited in the ProteomeXchange Consortium via the iProX partner repository^{47,48} under accession code [PXD051809](#). All other data are available within this Article and Supplementary Files. Source data are provided with this paper.

References

- Keenan, E. K., Zachman, D. K. & Hirshey, M. D. Discovering the landscape of protein modifications. *Mol. Cell* **81**, 1868–1878 (2021).
- Hitosugi, T. & Chen, J. Post-translational modifications and the Warburg effect. *Oncogene* **33**, 4279–4285 (2014).
- Deribe, Y. L., Pawson, T. & Dikic, I. Post-translational modifications in signal integration. *Nat. Struct. Mol. Biol.* **17**, 666–672 (2010).
- Choudhary, C., Weinert, B. T., Nishida, Y., Verdin, E. & Mann, M. The growing landscape of lysine acetylation links metabolism and cell signalling. *Nat. Rev. Mol. Cell Biol.* **15**, 536–550 (2014).
- Swatek, K. N. & Komander, D. Ubiquitin modifications. *Cell Res.* **26**, 399–422 (2016).
- Ubersax, J. A. & Ferrell, J. E. Jr. Mechanisms of specificity in protein phosphorylation. *Nat. Rev. Mol. Cell Biol.* **8**, 530–541 (2007).
- Zhang, Z. et al. Identification of lysine succinylation as a new post-translational modification. *Nat. Chem. Biol.* **7**, 58–63 (2011).
- Yang, Z. et al. Lactylome analysis suggests lactylation-dependent mechanisms of metabolic adaptation in hepatocellular carcinoma. *Nat. Metab.* **5**, 61–79 (2023).
- Tan, M. et al. Identification of 67 histone marks and histone lysine crotonylation as a new type of histone modification. *Cell* **146**, 1016–1028 (2011).
- Sabari, B. R. et al. Intracellular crotonyl-CoA stimulates transcription through p300-catalyzed histone crotonylation. *Mol. Cell* **58**, 203–215 (2015).
- Liu, X. et al. MOF as an evolutionarily conserved histone crotonyltransferase and transcriptional activation by histone acetyltransferase-deficient and crotonyltransferase-competent CBP/p300. *Cell Discov.* **3**, 17016 (2017).
- Wei, W. et al. Class I histone deacetylases are major histone decrotonylases: evidence for critical and broad function of histone crotonylation in transcription. *Cell Res.* **27**, 898–915 (2017).
- Bao, X. et al. Identification of ‘erasers’ for lysine crotonylated histone marks using a chemical proteomics approach. *Elife* **3**, e02999 (2014).
- Kollenstart, L. et al. Gcn5 and Esa1 function as histone crotonyltransferases to regulate crotonylation-dependent transcription. *J. Biol. Chem.* **294**, 20122–20134 (2019).
- Liu, S. et al. Chromodomain protein CDYL acts as a crotonyl-CoA hydratase to regulate histone crotonylation and spermatogenesis. *Mol. Cell* **67**, 853–866.e855 (2017).
- Jiang, G. et al. HIV latency is reversed by ACSS2-driven histone crotonylation. *J. Clin. Invest.* **128**, 1190–1198 (2018).
- Tang, X. et al. Short-chain enoyl-CoA hydratase mediates histone crotonylation and contributes to cardiac homeostasis. *Circulation* **143**, 1066–1069 (2021).
- Xu, W. et al. Global profiling of crotonylation on non-histone proteins. *Cell Res.* **27**, 946–949 (2017).
- Yu, H. et al. Global crotonylome reveals CDYL-regulated RPA1 crotonylation in homologous recombination-mediated DNA repair. *Sci. Adv.* **6**, eaay4697 (2020).
- Warburg, O. On the origin of cancer cells. *Science* **123**, 309–314 (1956).
- Liberti, M. V. & Locasale, J. W. The Warburg effect: how does it benefit cancer cells? *Trends Biochem. Sci.* **41**, 211–218 (2016).
- DeBerardinis, R. J., Lum, J. J., Hatzivassiliou, G. & Thompson, C. B. The biology of cancer: metabolic reprogramming fuels cell growth and proliferation. *Cell Metab.* **7**, 11–20 (2008).
- Lunt, S. Y. & Vander Heiden, M. G. Aerobic glycolysis: meeting the metabolic requirements of cell proliferation. *Annu. Rev. Cell Dev. Biol.* **27**, 441–464 (2011).
- Schito, L. & Rey, S. Cell-autonomous metabolic reprogramming in hypoxia. *Trends Cell Biol.* **28**, 128–142 (2018).
- Xie, H. & Simon, M. C. Oxygen availability and metabolic reprogramming in cancer. *J. Biol. Chem.* **292**, 16825–16832 (2017).
- Kim, J. W., Tchernyshyov, I., Semenza, G. L. & Dang, C. V. HIF-1-mediated expression of pyruvate dehydrogenase kinase: a metabolic switch required for cellular adaptation to hypoxia. *Cell Metab.* **3**, 177–185 (2006).
- Papandreou, I., Cairns, R. A., Fontana, L., Lim, A. L. & Denko, N. C. HIF-1 mediates adaptation to hypoxia by actively downregulating mitochondrial oxygen consumption. *Cell Metab.* **3**, 187–197 (2006).
- Wang, H. J. et al. JMJD5 regulates PKM2 nuclear translocation and reprograms HIF-1 α -mediated glucose metabolism. *Proc. Natl. Acad. Sci. USA* **111**, 279–284 (2014).
- Boidot, R. et al. Regulation of monocarboxylate transporter MCT1 expression by p53 mediates inward and outward lactate fluxes in tumors. *Cancer Res.* **72**, 939–948 (2012).
- Fellows, R. et al. Microbiota derived short chain fatty acids promote histone crotonylation in the colon through histone deacetylases. *Nat. Commun.* **9**, 105 (2018).
- Schito, L. & Semenza, G. L. Hypoxia-inducible factors: master regulators of cancer progression. *Trends Cancer* **2**, 758–770 (2016).

32. Semenza, G. L. Hypoxia-inducible factors in physiology and medicine. *Cell* **148**, 399–408 (2012).
 33. Qian, X. et al. Phosphoglycerate kinase 1 phosphorylates beclin1 to induce autophagy. *Mol. Cell* **65**, 917–931.e916 (2017).
 34. Li, X. et al. Mitochondria-translocated PGK1 functions as a protein kinase to coordinate glycolysis and the TCA cycle in tumorigenesis. *Mol. Cell* **61**, 705–719 (2016).
 35. Ji, Y. et al. Adenylate kinase hCINAP determines self-renewal of colorectal cancer stem cells by facilitating LDHA phosphorylation. *Nat. Commun.* **8**, 15308 (2017).
 36. Hirschhaeuser, F., Sattler, U. G. & Mueller-Klieser, W. Lactate: a metabolic key player in cancer. *Cancer Res.* **71**, 6921–6925 (2011).
 37. Tang, S. J. et al. Phosphoglycerate kinase 1-overexpressing lung cancer cells reduce cyclooxygenase 2 expression and promote anti-tumor immunity in vivo. *Int. J. Cancer* **123**, 2840–2848 (2008).
 38. Ding, H. et al. Phosphoglycerate kinase 1 promotes radioresistance in U251 human glioma cells. *Oncol. Rep.* **31**, 894–900 (2014).
 39. Li, X., Zheng, Y. & Lu, Z. PGK1 is a new member of the protein kinome. *Cell Cycle* **15**, 1803–1804 (2016).
 40. Martinez-Reyes, I. & Chandel, N. S. Cancer metabolism: looking forward. *Nat. Rev. Cancer* **21**, 669–680 (2021).
 41. Zhang, Y. et al. Macrophage-associated PGK1 phosphorylation promotes aerobic glycolysis and tumorigenesis. *Mol. Cell* **71**, 201–215.e207 (2018).
 42. Wang, S. et al. Insulin and mTOR pathway regulate HDAC3-mediated deacetylation and activation of PGK1. *PLoS Biol.* **13**, e1002243 (2015).
 43. Hu, H. et al. Acetylation of PGK1 promotes liver cancer cell proliferation and tumorigenesis. *Hepatology* **65**, 515–528 (2017).
 44. Nie, H. et al. O-GlcNAcylation of PGK1 coordinates glycolysis and TCA cycle to promote tumor growth. *Nat. Commun.* **11**, 36 (2020).
 45. Yang, C. et al. De novo pyrimidine biosynthetic complexes support cancer cell proliferation and ferroptosis defence. *Nat. Cell Biol.* **25**, 836–847 (2023).
 46. Tang, Z. et al. GEPIA: a web server for cancer and normal gene expression profiling and interactive analyses. *Nucleic Acids Res.* **45**, W98–W102 (2017).
 47. Ma, J. et al. iProX: an integrated proteome resource. *Nucleic Acids Res.* **47**, D1211–D1217 (2019).
 48. Chen, T. et al. iProX in 2021: connecting proteomics data sharing with big data. *Nucleic Acids Res.* **50**, D1522–D1527 (2022).
- and MS. This study was supported by grants from the National Natural Science Foundation of China (82372634 to C.Y.; 82325038 and 82030093 to B.L.), Beijing Natural Science Foundation (5194023 to C.Y.) and Key R&D Program of Zhejiang (2024SSYS0034 to C.Y.).

Author contributions

C.Y. and B.L. conceived and designed the study; Z.G. and C.Y. performed the experiments and analyzed the results with contributions from Y.Z., H.W., L.L., L.M., Y.L.Z., R.Y., X.L., J.N., Q.C. and Y.F.; C.Y. and Z.G. wrote the paper; and all authors read and approved the manuscript.

Competing interests

The authors declare no competing interests.

Additional information

Supplementary information The online version contains supplementary material available at <https://doi.org/10.1038/s41467-024-51232-w>.

Correspondence and requests for materials should be addressed to Binghui Li or Chuanzhen Yang.

Peer review information *Nature Communications* thanks Lei Jiang and the other anonymous reviewer(s) for their contribution to the peer review of this work. A peer review file is available.

Reprints and permissions information is available at <http://www.nature.com/reprints>

Publisher's note Springer Nature remains neutral with regard to jurisdictional claims in published maps and institutional affiliations.

Open Access This article is licensed under a Creative Commons Attribution-NonCommercial-NoDerivatives 4.0 International License, which permits any non-commercial use, sharing, distribution and reproduction in any medium or format, as long as you give appropriate credit to the original author(s) and the source, provide a link to the Creative Commons licence, and indicate if you modified the licensed material. You do not have permission under this licence to share adapted material derived from this article or parts of it. The images or other third party material in this article are included in the article's Creative Commons licence, unless indicated otherwise in a credit line to the material. If material is not included in the article's Creative Commons licence and your intended use is not permitted by statutory regulation or exceeds the permitted use, you will need to obtain permission directly from the copyright holder. To view a copy of this licence, visit <http://creativecommons.org/licenses/by-nc-nd/4.0/>.

© The Author(s) 2024

Acknowledgements

We thank the Metabolomics Facility Center of Metabolomics and Lipidomics at the National Protein Science Technology Center of Tsinghua University for LC-MS/MS experiments. We also thank Jun Deng and Jia Hu (Core Facilities of Basic Medical Sciences of Capital Medical University), and Xue Bai (Mass Spectrometry & Metabolomics Core Facility of Westlake University) for their assistance with microscopic imaging